**Supporting Information**

# Near-infrared phosphorescence in a ruthenium(II) complex equipped with a pyridyl-1,2-azaborine ligand

Matteo Pompei,[a] Filippo Monti,*[b] Letizia Sambri,[a] Nicola Armaroli [b] and Andrea Baschieri *[b]

[a] Department of Industrial Chemistry "Toso Montanari", University of Bologna, Via Piero Gobetti 85, 40129 Bologna, Italy.

[b] Institute for Organic Synthesis and Photoreactivity (ISOF), National Research Council of Italy (CNR), Via Piero Gobetti 101, 40129 Bologna, Italy.

E-mail: F. M.: filippo.monti@isof.cnr.it
A. B.: andrea.baschieri@isof.cnr.it

## Table of Contents

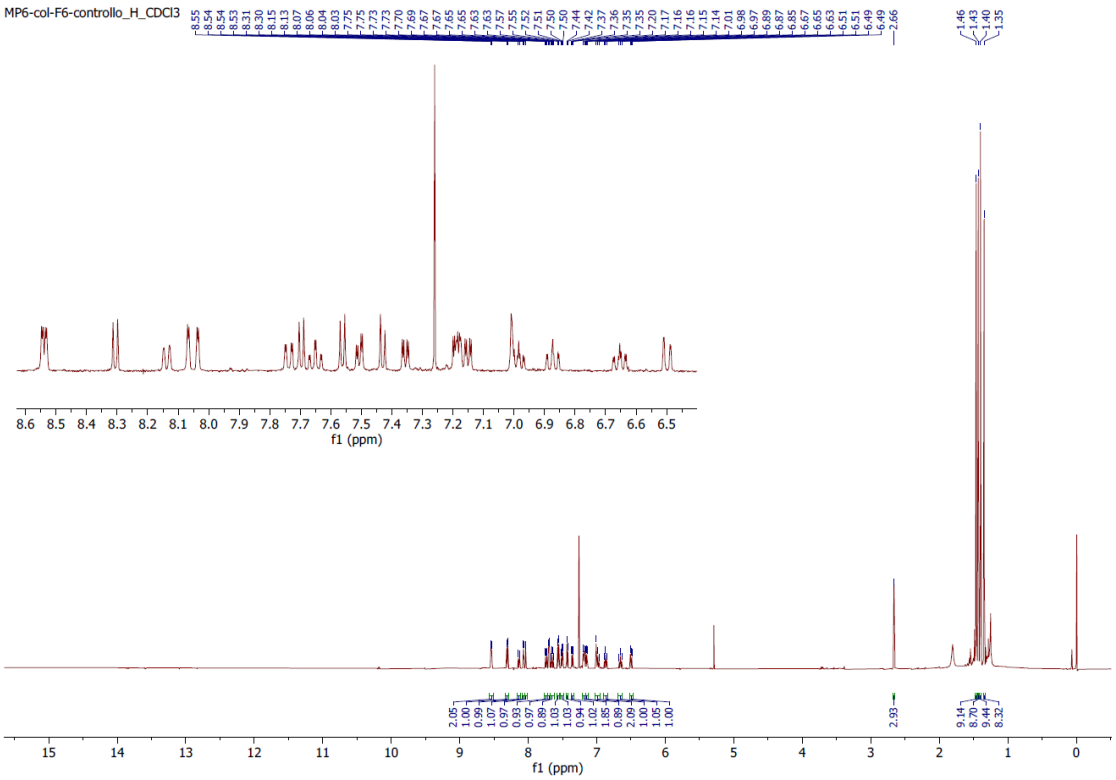


**Figure S1.** $^{1}H$ NMR spectrum of complex **A** in $CDCl_3$.

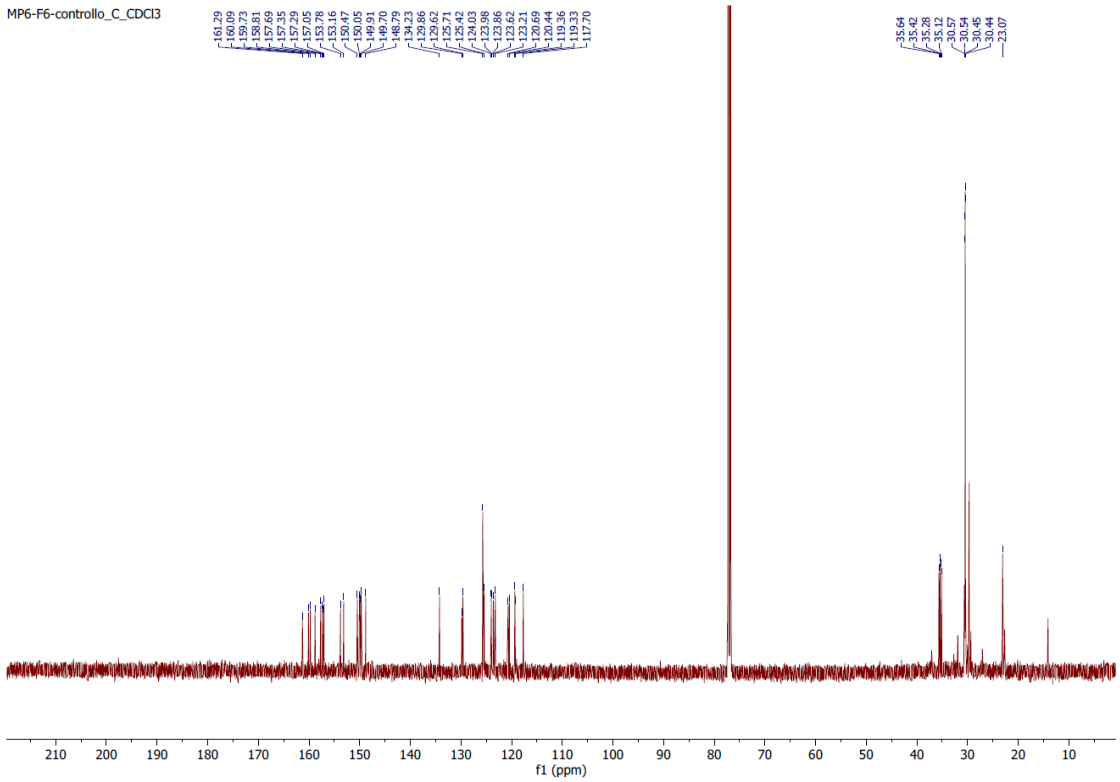


**Figure S2.** $^{13}C$ $\{^{1}H\}$ NMR spectrum of complex **A** in $CDCl_3$.

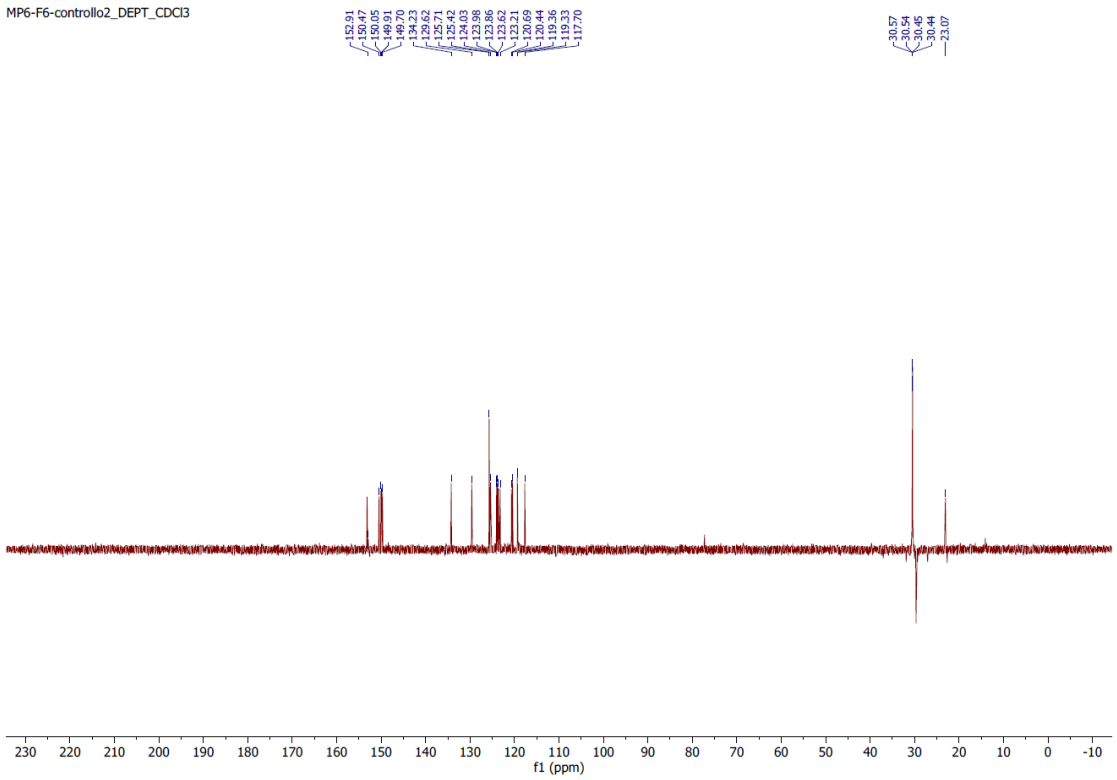


**Figure S3.** DEPT 135 {$^1$H} NMR spectrum of complex **A** in $CDCl_3$.

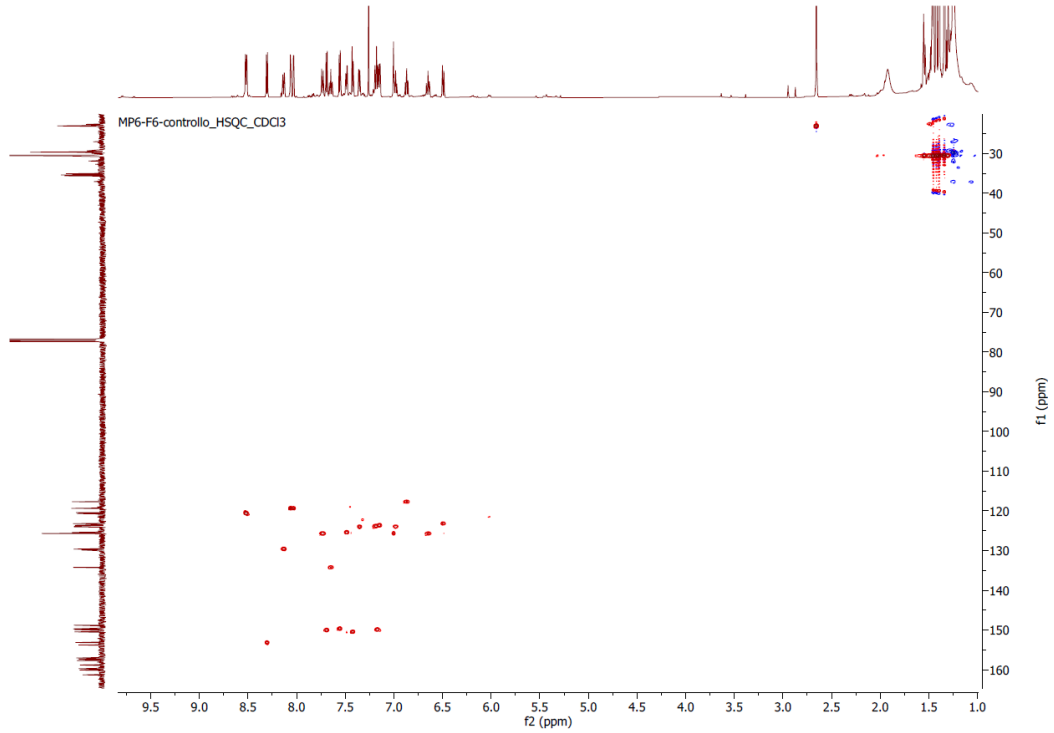


**Figure S4.** HSQC NMR spectrum of complex **A** in $CDCl_3$.

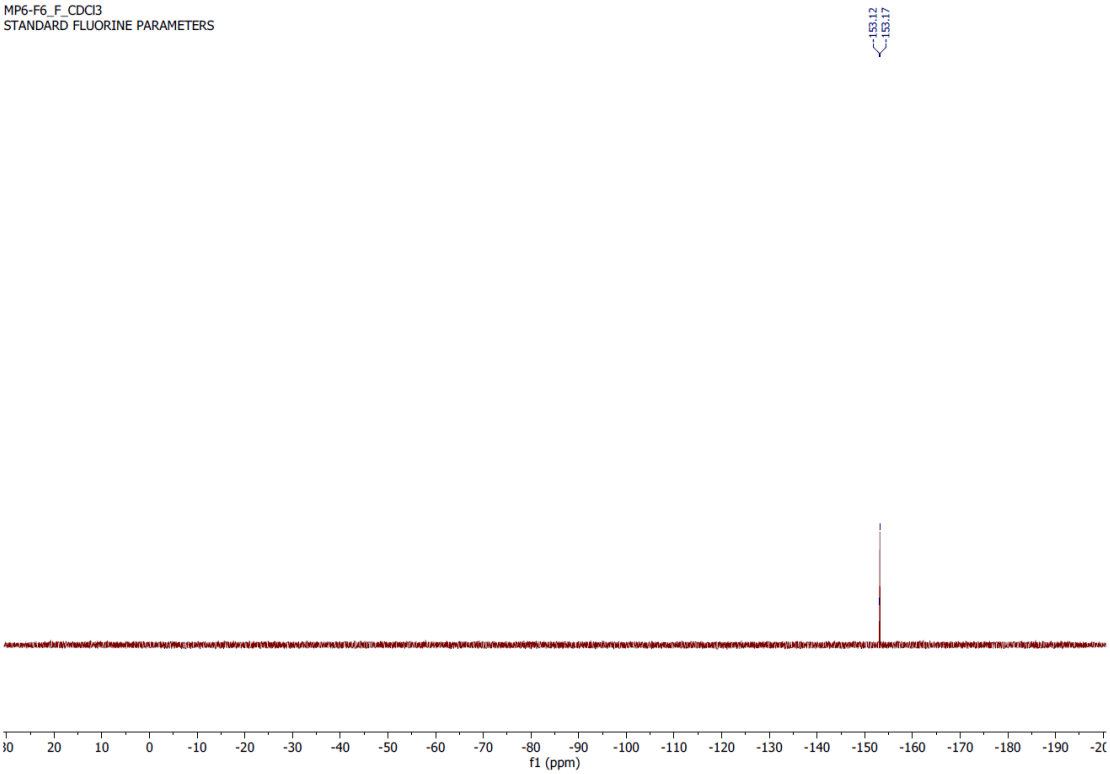


**Figure S5.** $^{19}F$ NMR spectrum of complex **A** in $CDCl_3$.

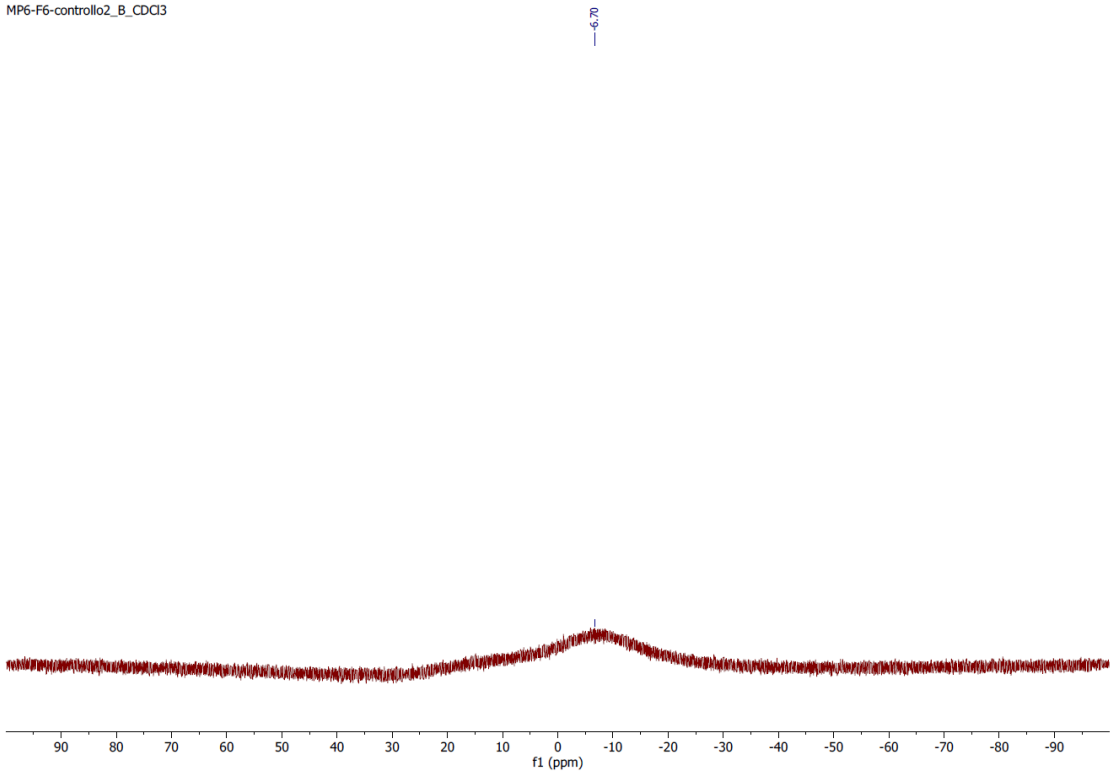


**Figure S6.** $^{11}B$ NMR spectrum of complex **A** in $CDCl_3$.

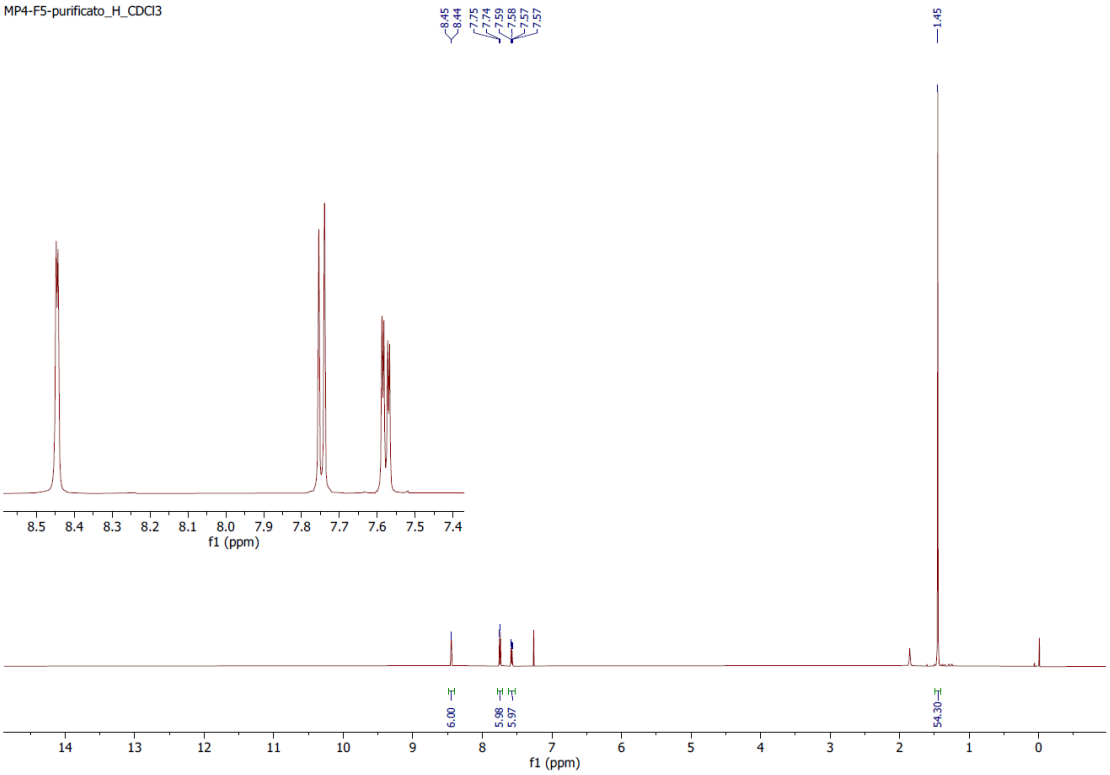


**Figure S7.** $^{1}$H NMR spectrum of complex **B** in $CDCl_3$.

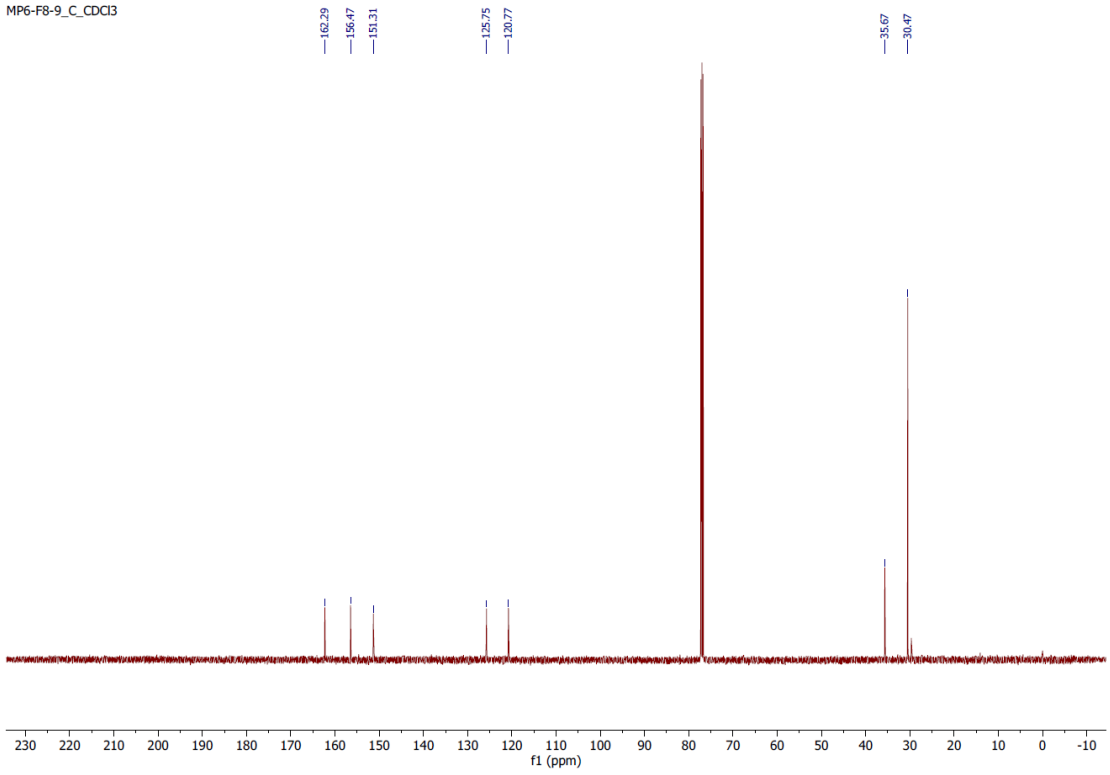


**Figure S8.** $^{13}$C {$^{1}$H} NMR spectrum of complex **B** in $CDCl_3$.

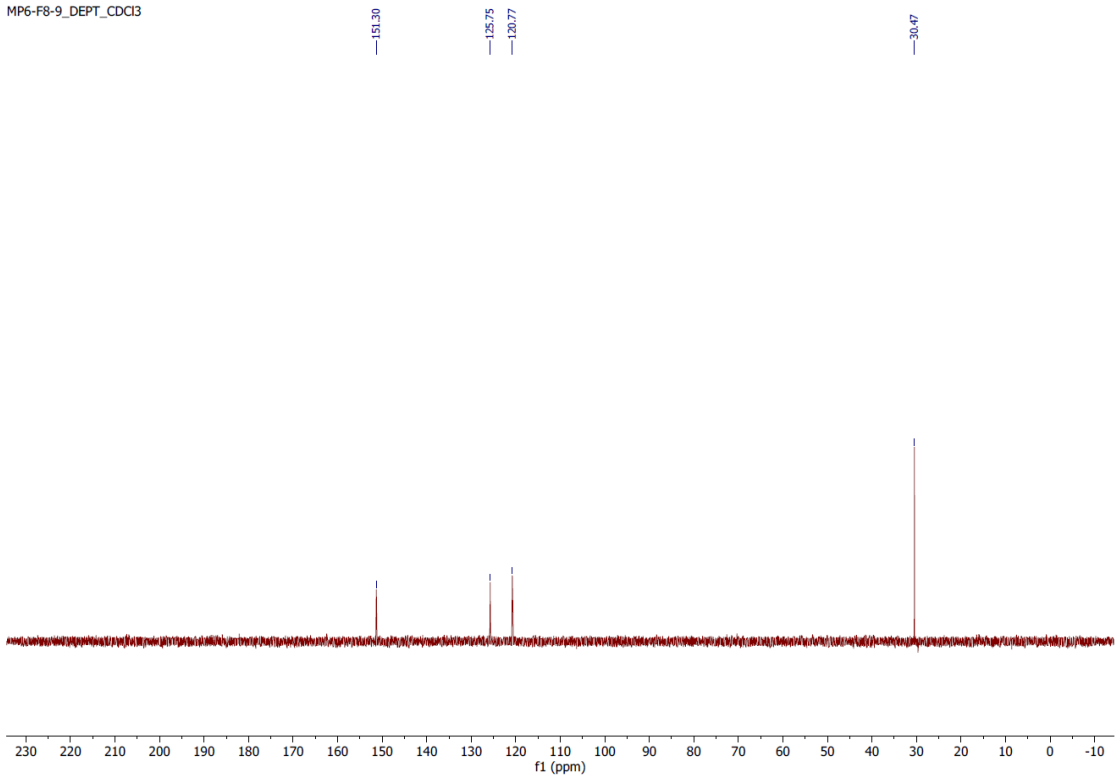


**Figure S9.** DEPT 135 {$^{1}$H} NMR spectrum of complex **B** in $CDCl_3$.

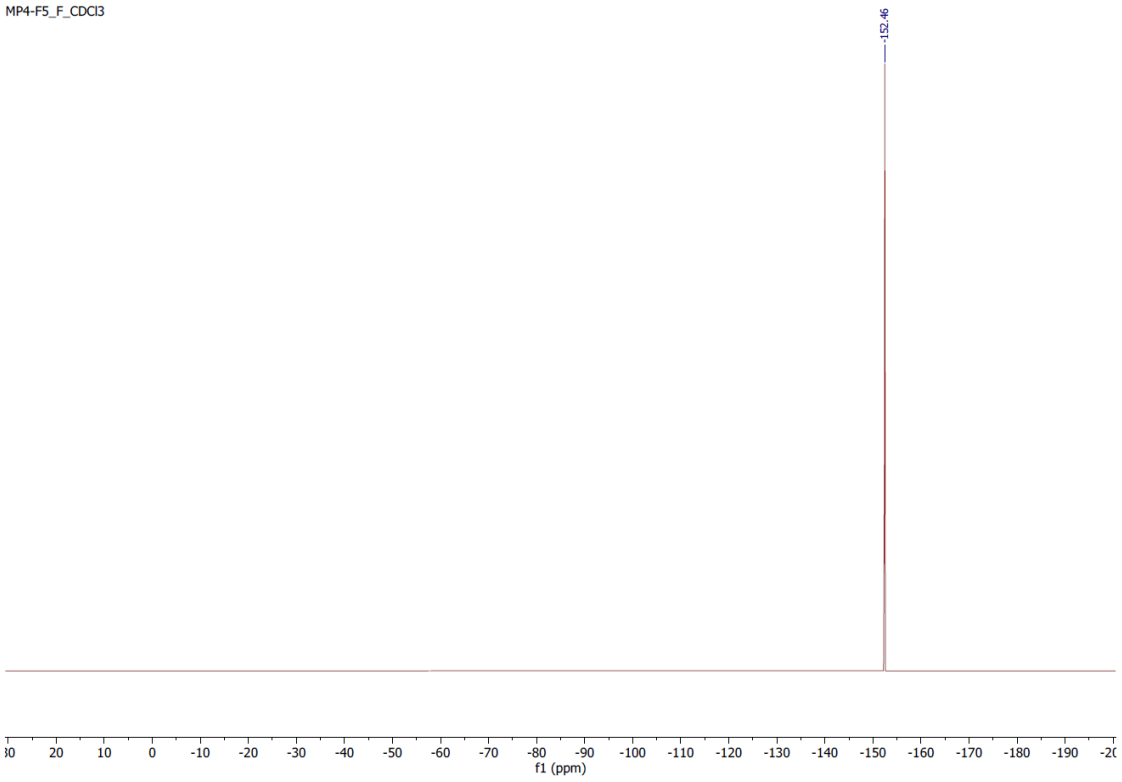


**Figure S10.** $^{19}$F NMR spectrum of complex **B** in $CDCl_3$.

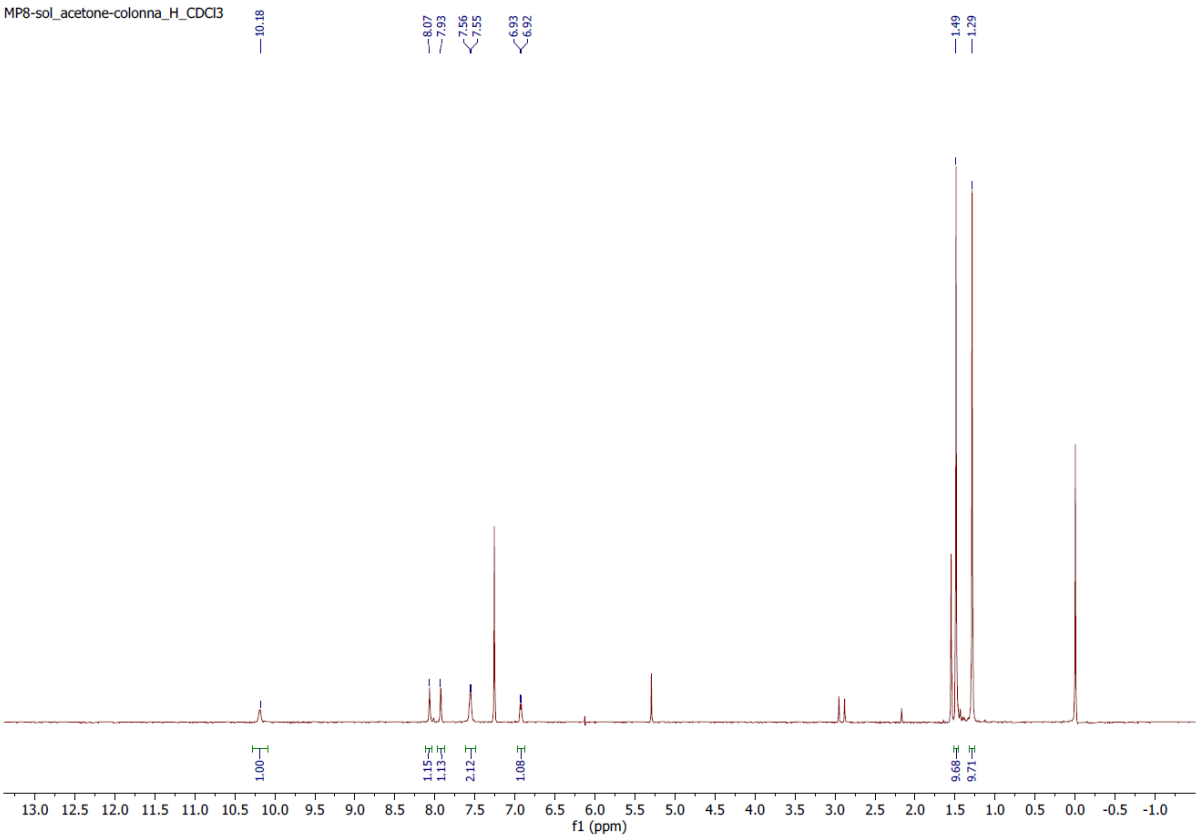


**Figure S11.** $^{1}$H NMR spectrum of precursor **[Ru(dtbpy)$_2$Cl$_2$]** in $CDCl_3$.

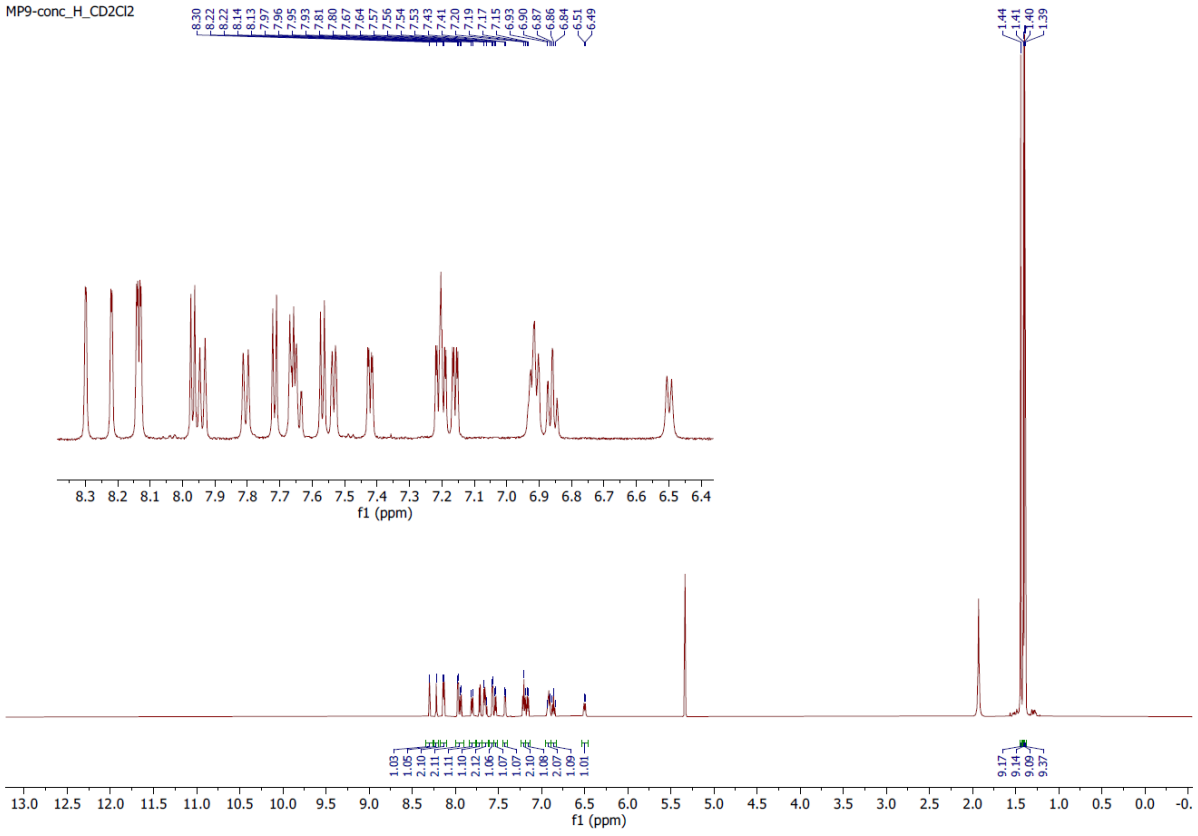


**Figure S12.** $^{1}$H NMR spectrum of complex **C** in $CD_2Cl_2$.

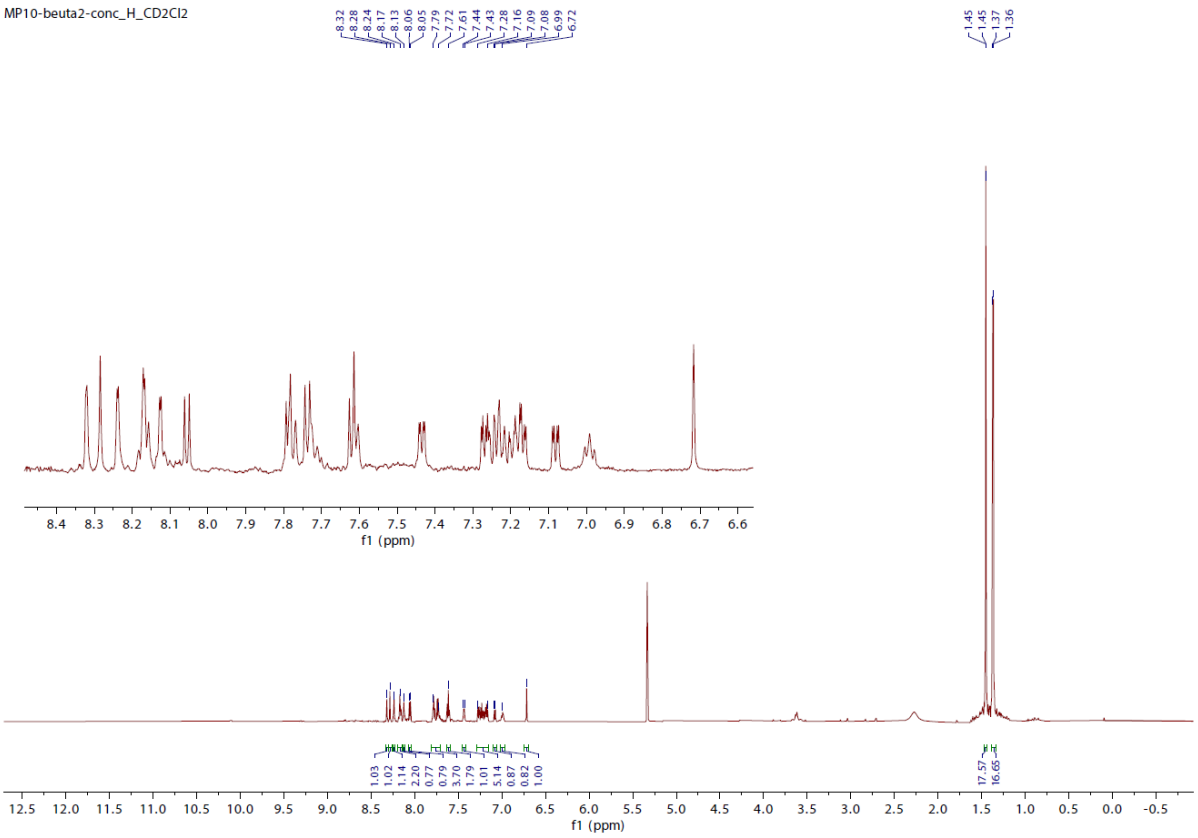


**Figure S13.** $^{1}H$ NMR spectrum of complex **D** in $CD_2Cl_2$.

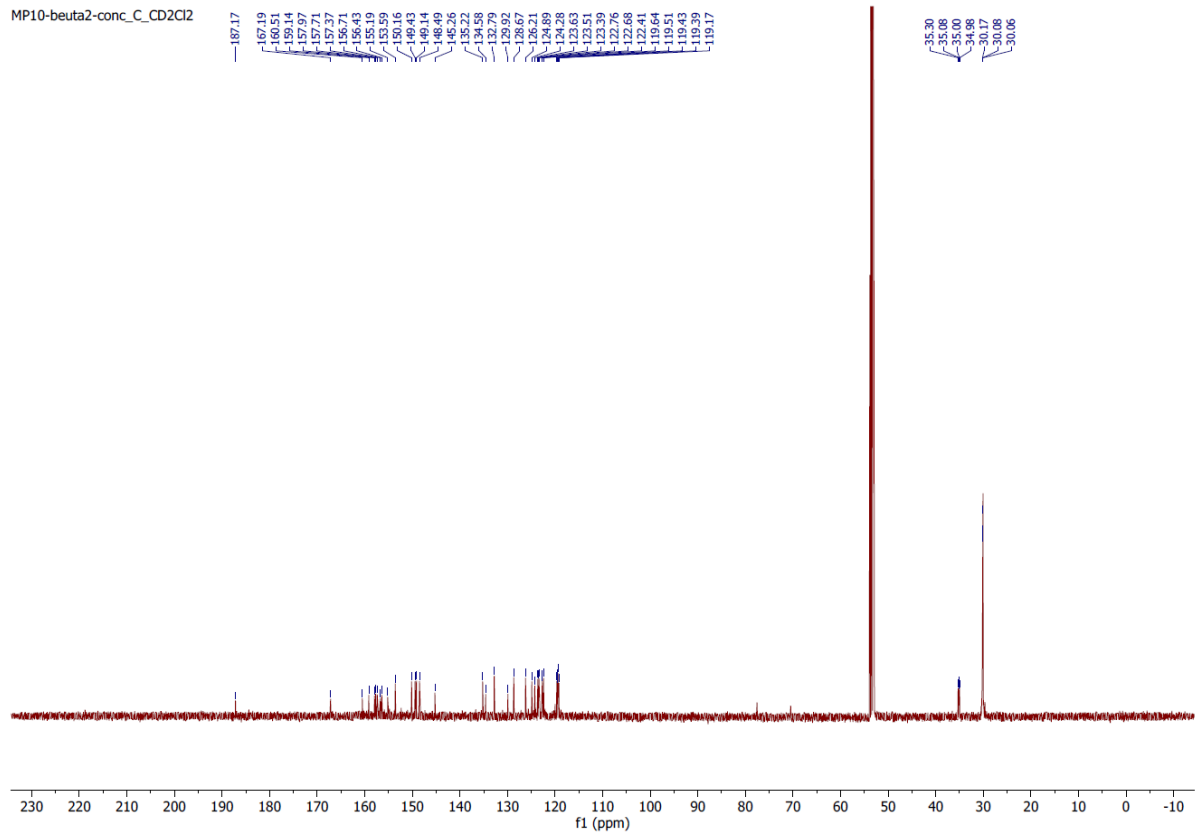


**Figure S14.** $^{13}C$ $\{^{1}H\}$ NMR spectrum of complex **D** in $CD_2Cl_2$.

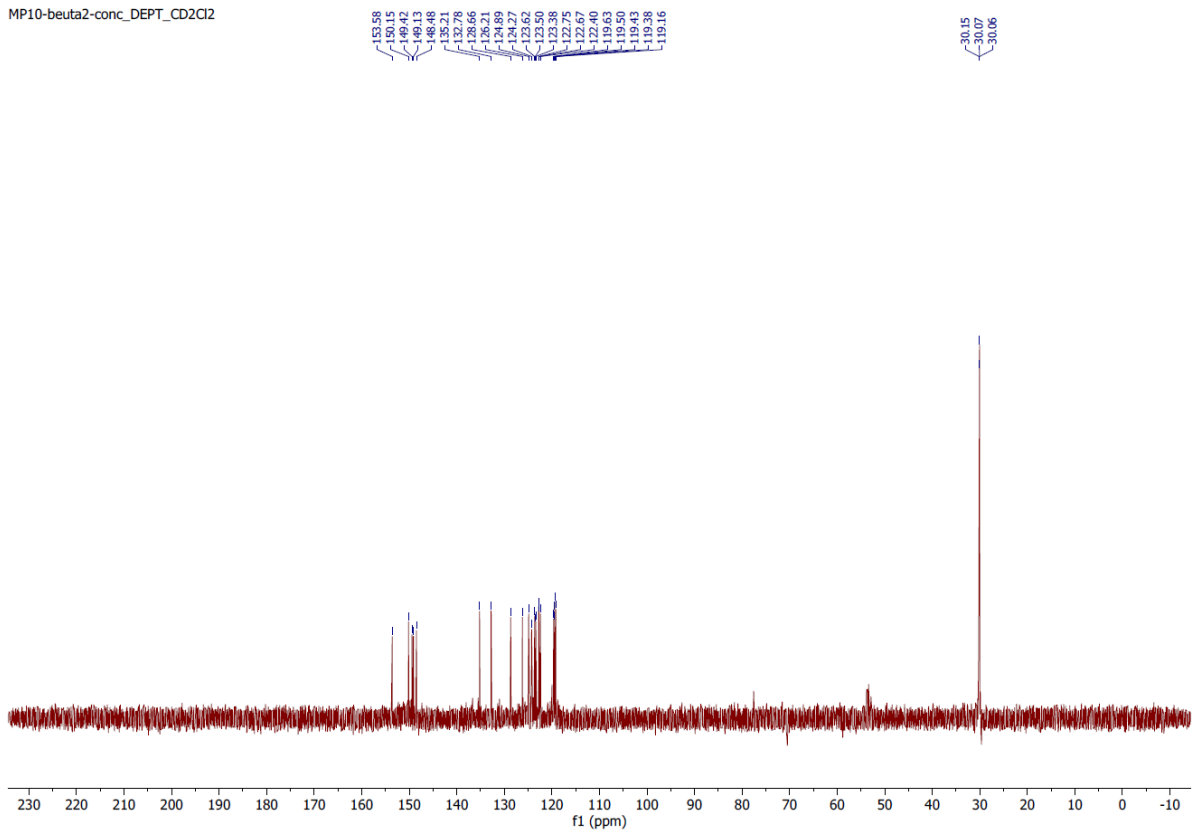


**Figure S15.** DEPT 135 {$^{1}$H} NMR spectrum of complex **D** in $CD_2Cl_2$.

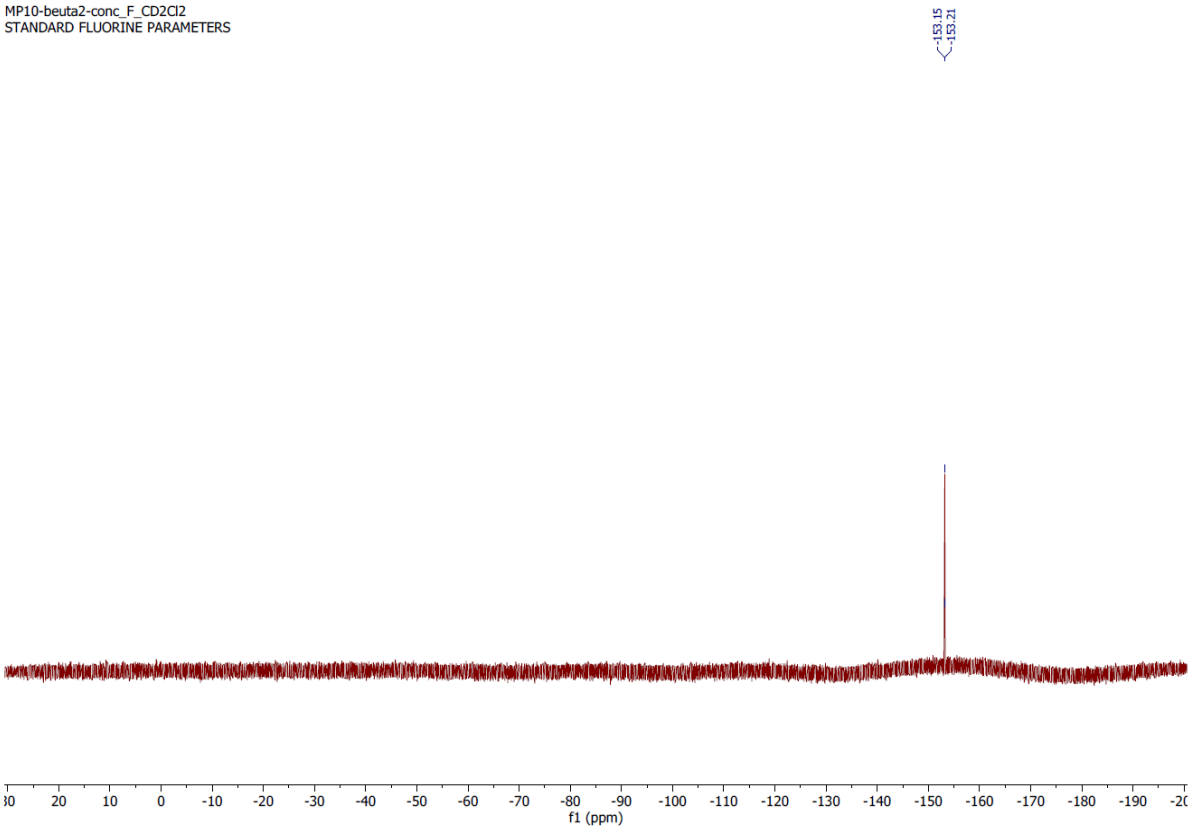


**Figure S16.** $^{19}$F NMR spectrum of complex **D** in $CD_2Cl_2$.

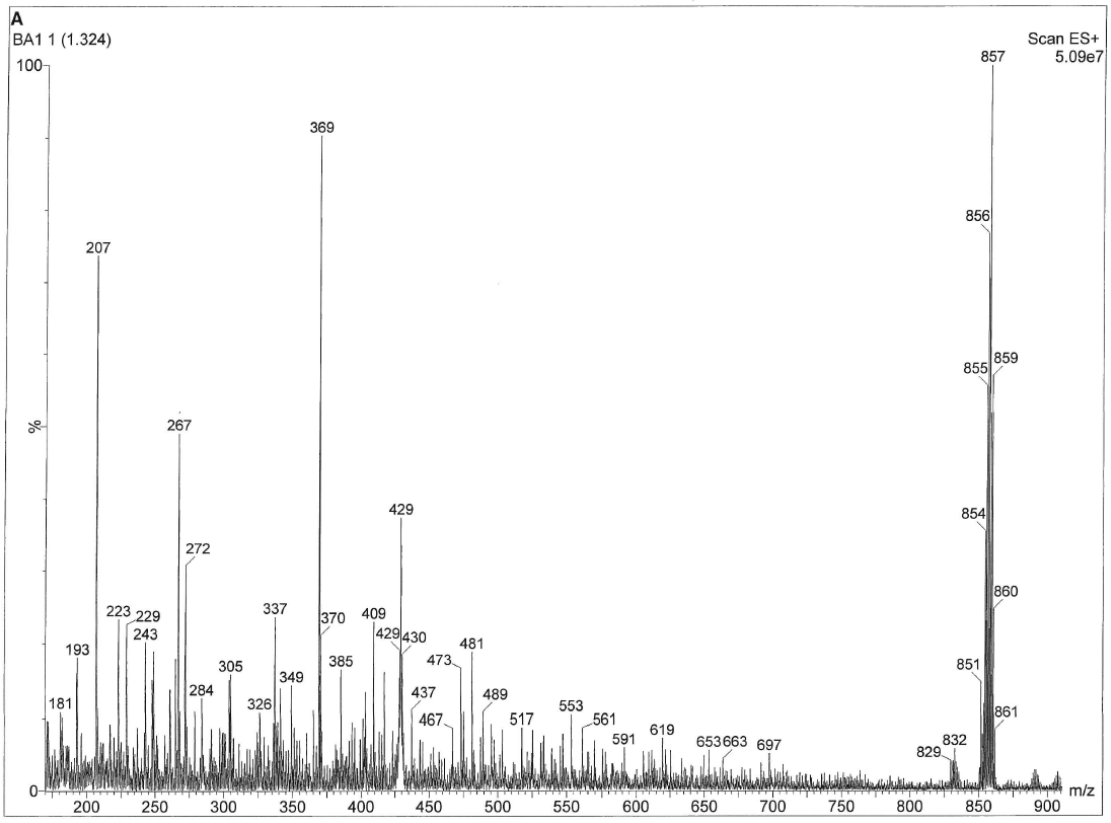


**Figure S17.** ESI$^+$ spectrum of complex **A**.

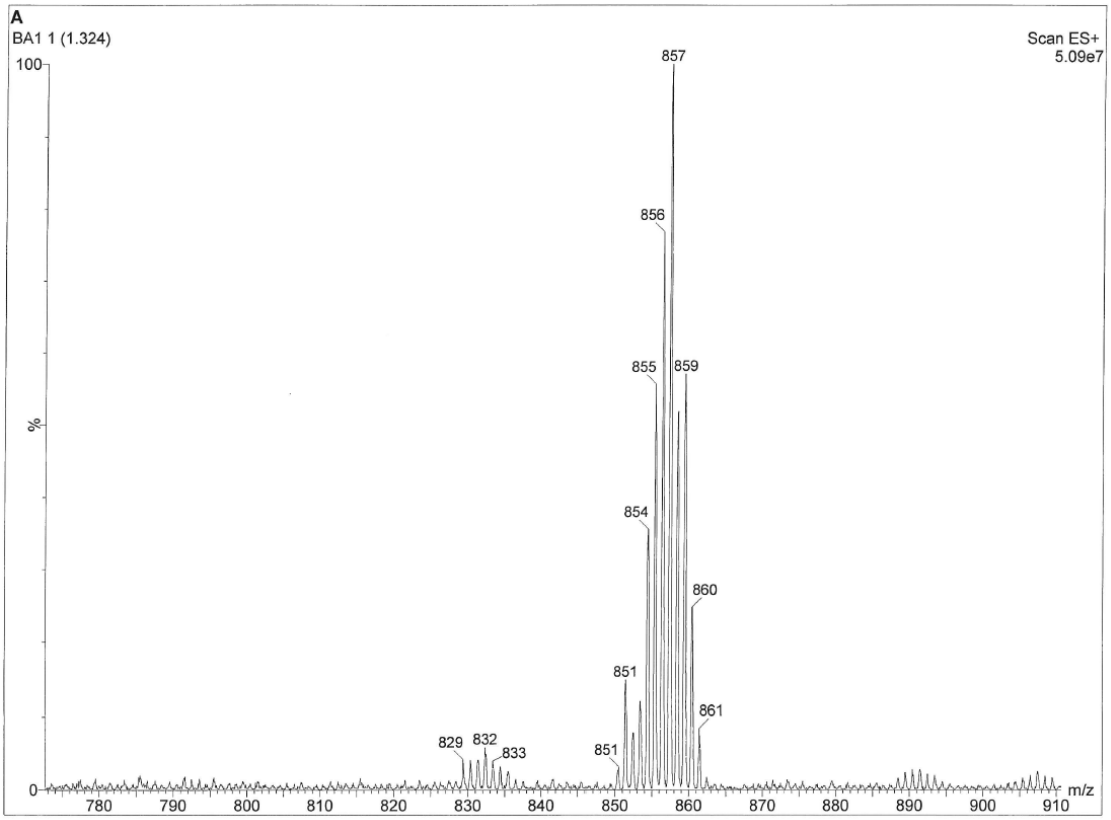


**Figure S18.** Detail of the ESI$^+$ spectrum of complex **A**.

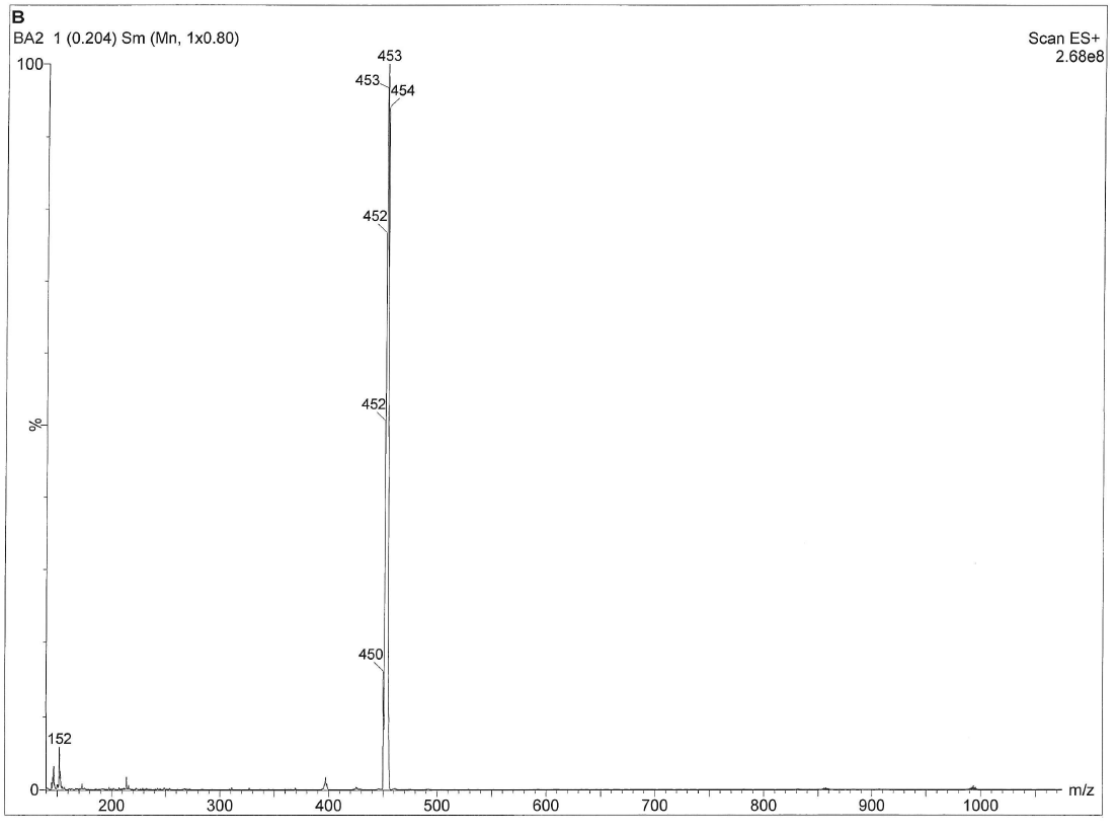


**Figure S19.** ESI$^+$ spectrum of complex **B**.

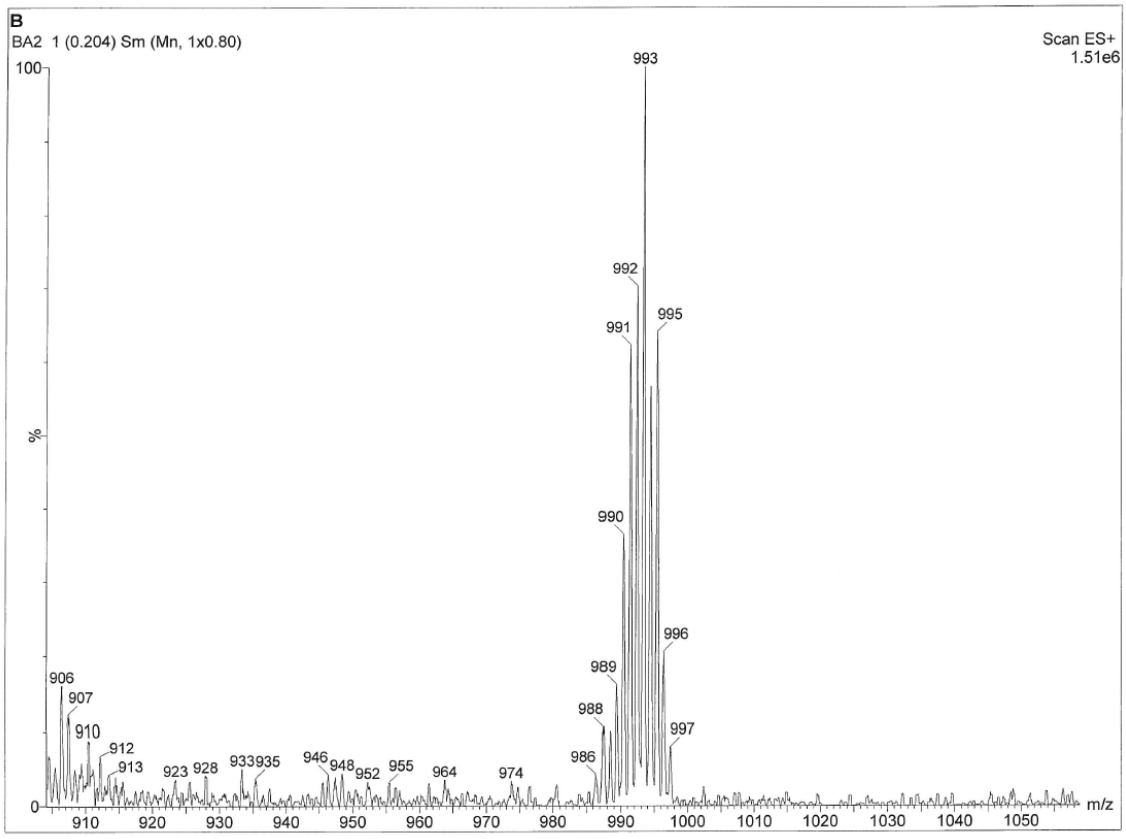


**Figure S20.** Detail of the ESI$^+$ spectrum of complex **B**.

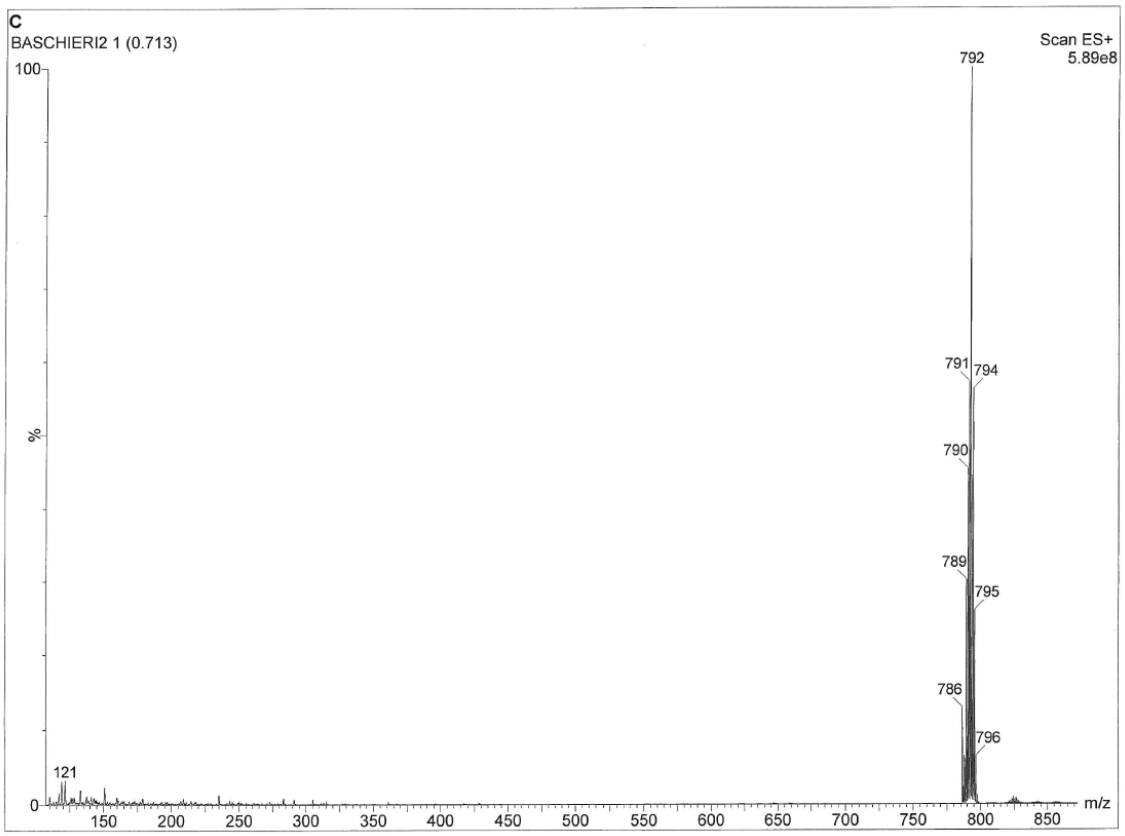


**Figure S21.** ESI$^+$ spectrum of complex **C**.

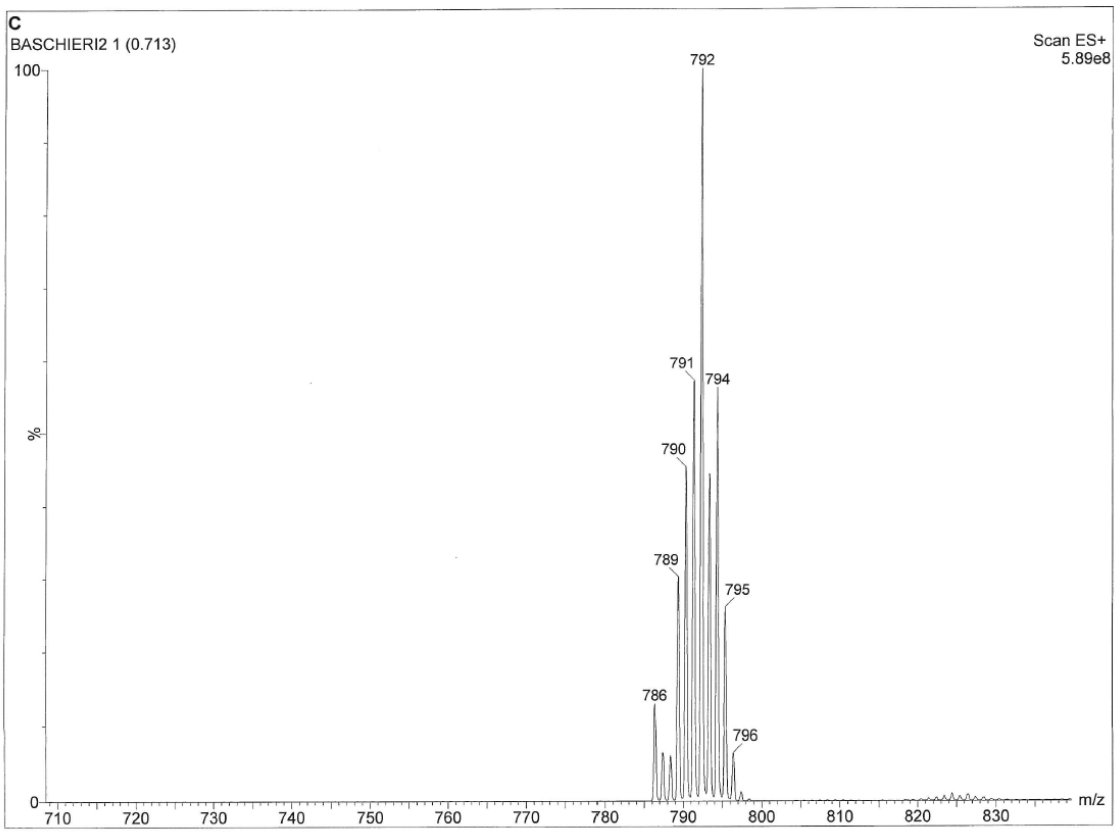


**Figure S22.** Detail of the ESI$^+$ spectrum of complex **C**.

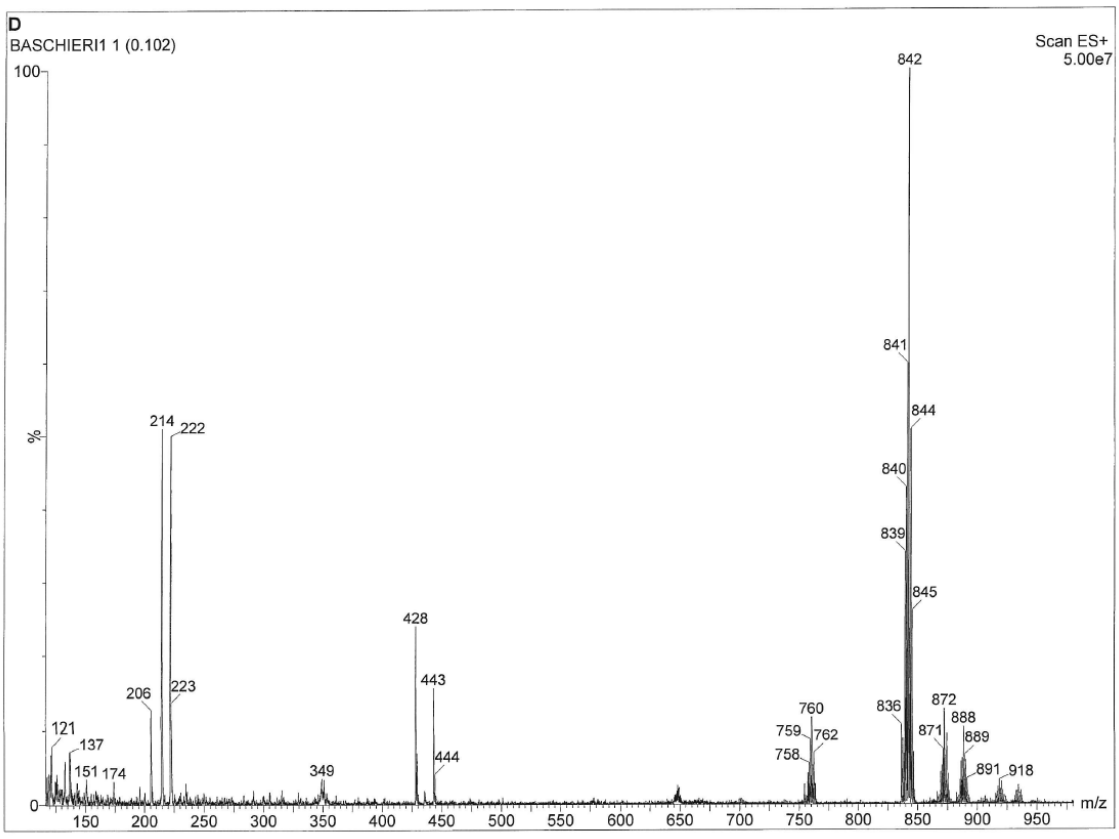


**Figure S23.** ESI$^+$ spectrum of complex **D**.

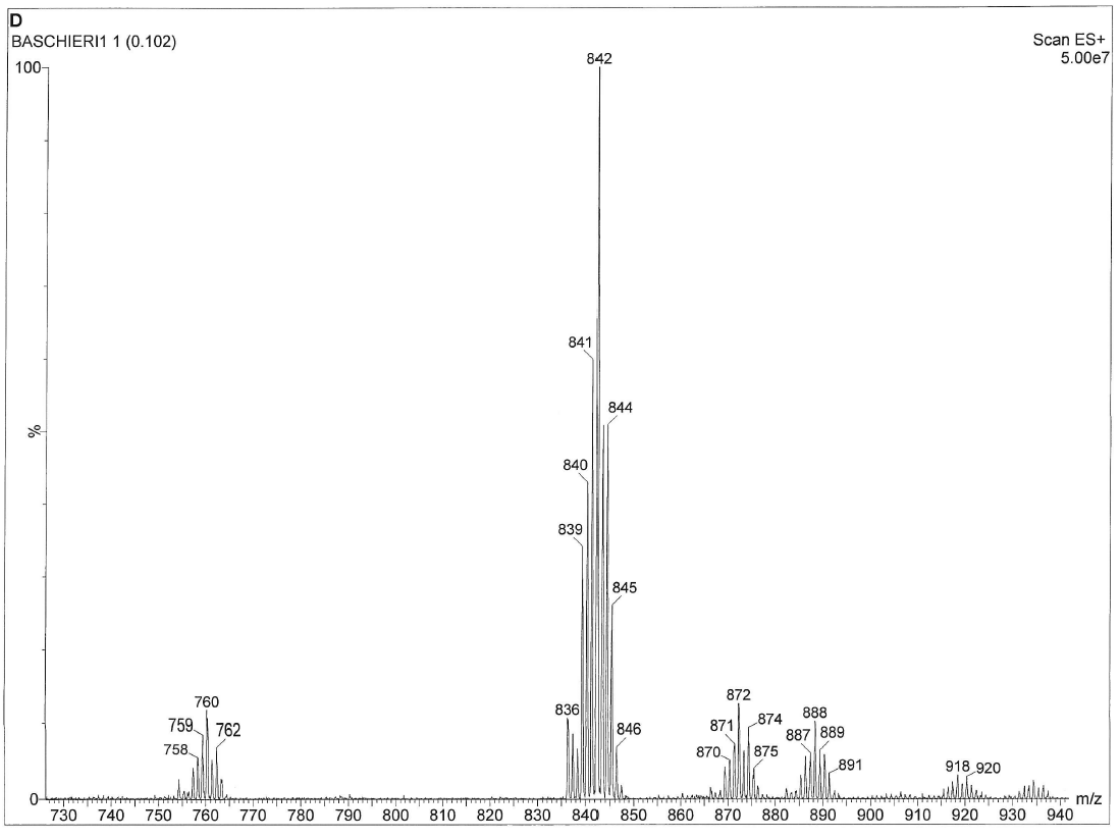


**Figure S24.** Detail of the ESI$^+$ spectrum of complex **D**.

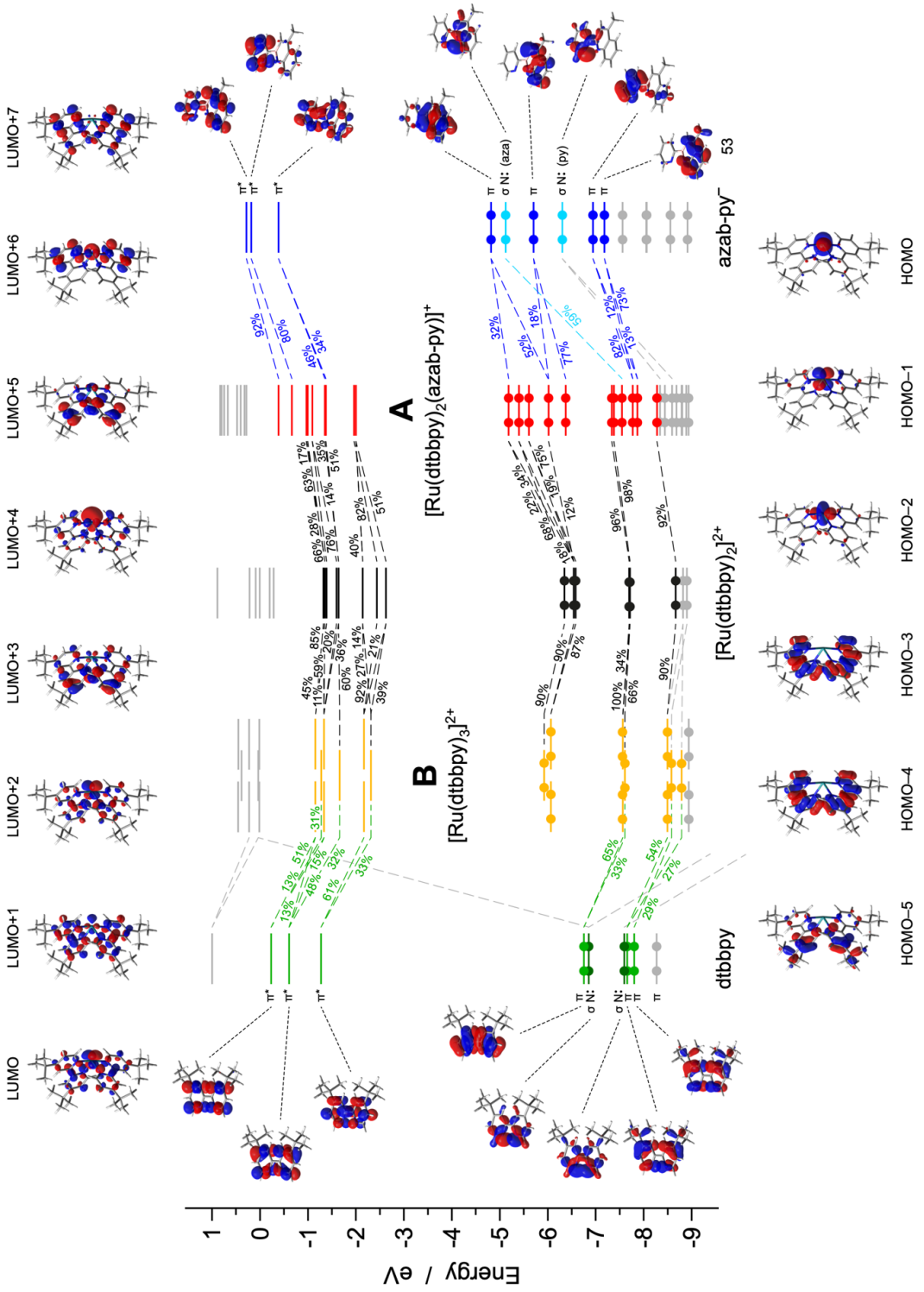


**Figure S25.** Orbital-interaction diagram of complexes **A** and **B**, calculated in acetonitrile using charge decomposition analysis (see Experimental Section for further details). Fragment orbitals are computed by dividing each complex into 2 fragments: the shared $[Ru(dtbbpy)_2]^{2+}$ moiety and the third N^N ligand (*i.e.*, another dtbbpy unit for **B** and the azaborine for **A**). Only fragment-orbital contributions above 10% are reported.

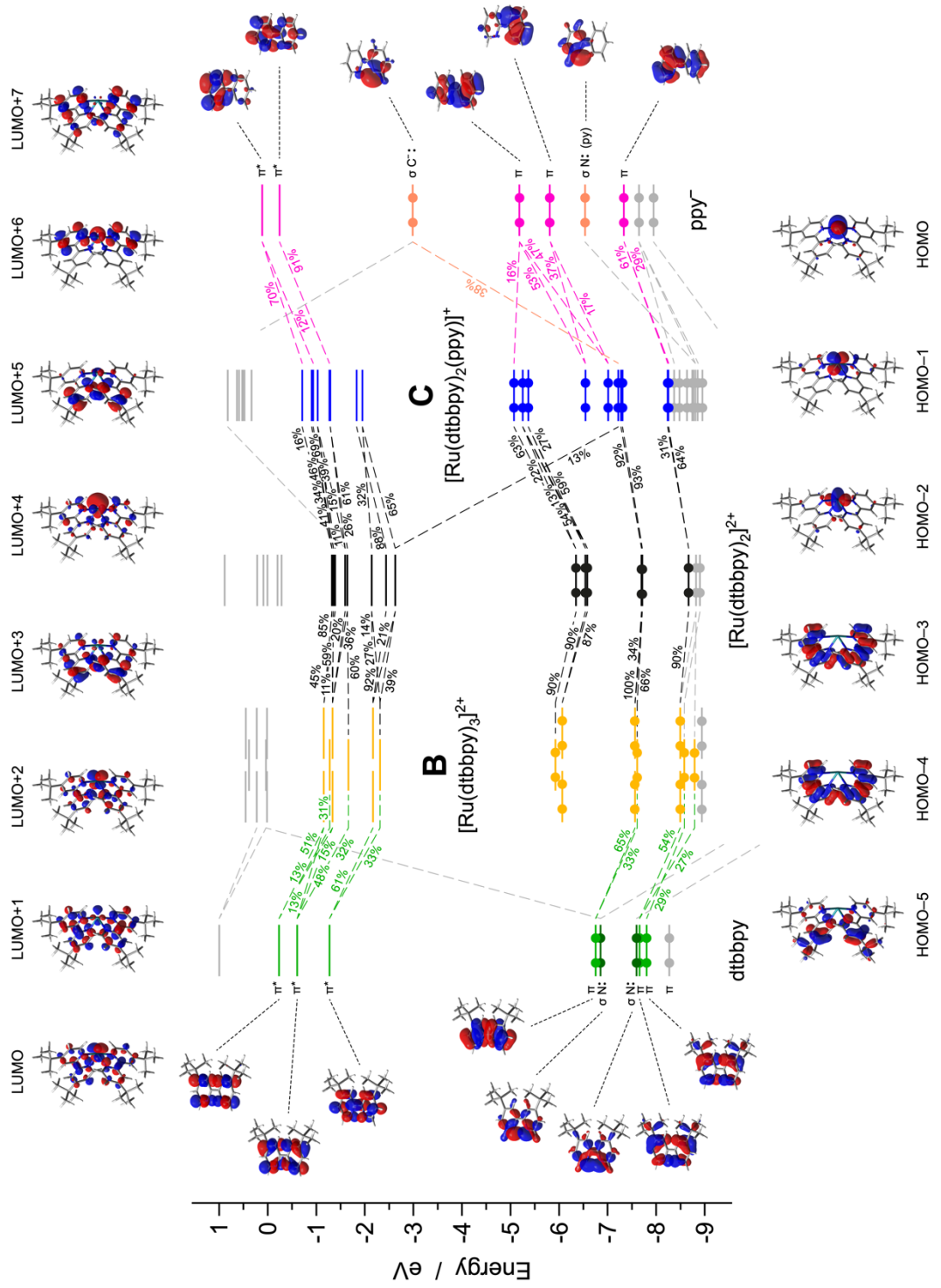


**Figure S26.** Orbital-interaction diagram of complexes **B** and **C**, calculated in acetonitrile using charge decomposition analysis (see Experimental Section for further details). Fragment orbitals are computed by dividing each complex into 2 fragments: the shared $[Ru(dtbbpy)_2]^{2+}$ moiety and the third ligand (*i.e.*, another dtbbpy unit for **B** and the anionic cyclometalating $ppy^-$ in the case of **C**). Only fragment-orbital contributions above 10% are reported.

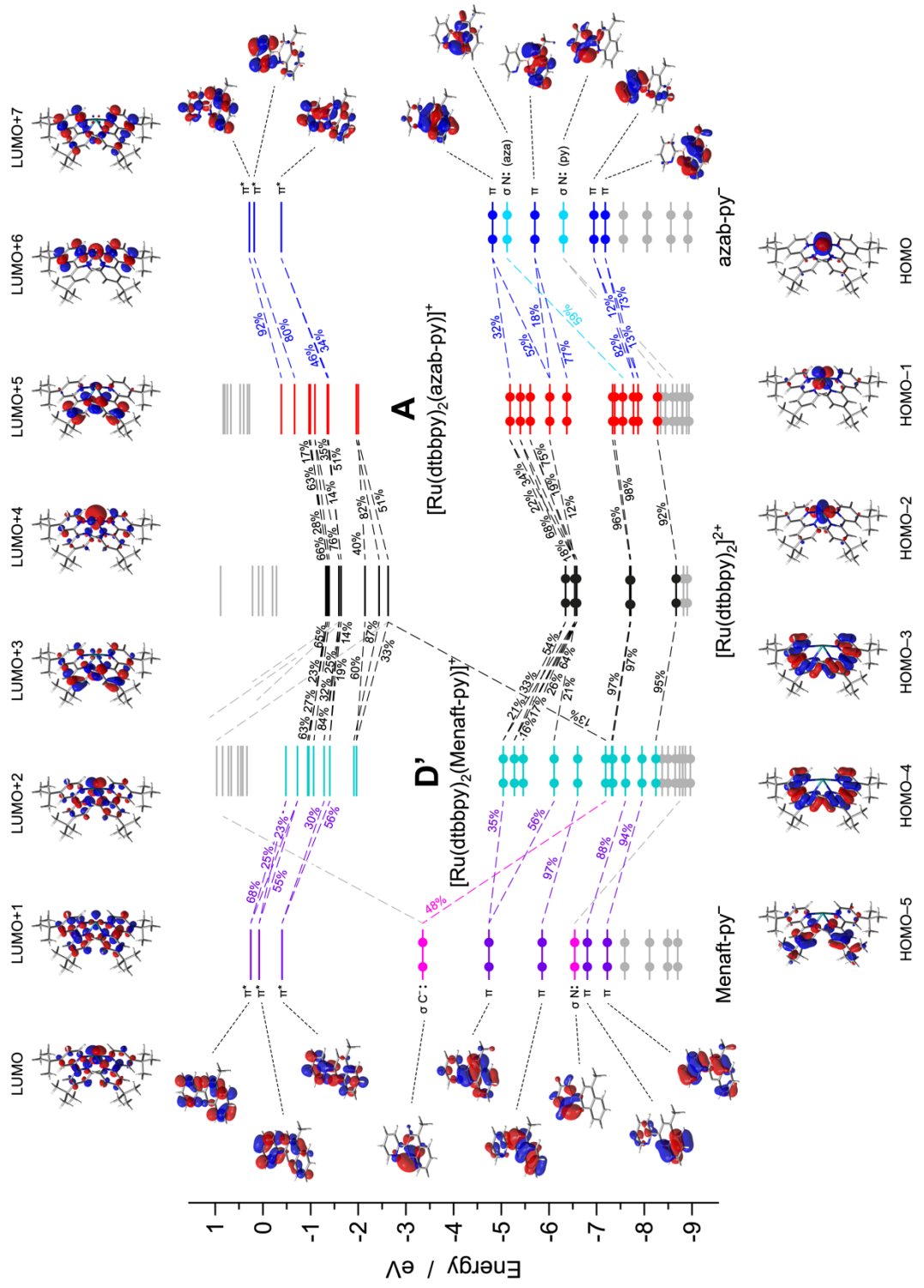


**Figure S27.** Orbital-interaction diagram of complexes **A** and **D'**, calculated in acetonitrile using charge decomposition analysis (see Experimental Section for further details). Fragment orbitals are computed by dividing each complex into 2 fragments: the shared $[Ru(dtbbpy)_2]^{2+}$ moiety and the anionic ligand (*i.e.*, the azaborine unit for **A** and the C=C counterpart for **D'**, which is just a theoretical construction). Only fragment-orbital contributions above 10% are reported.

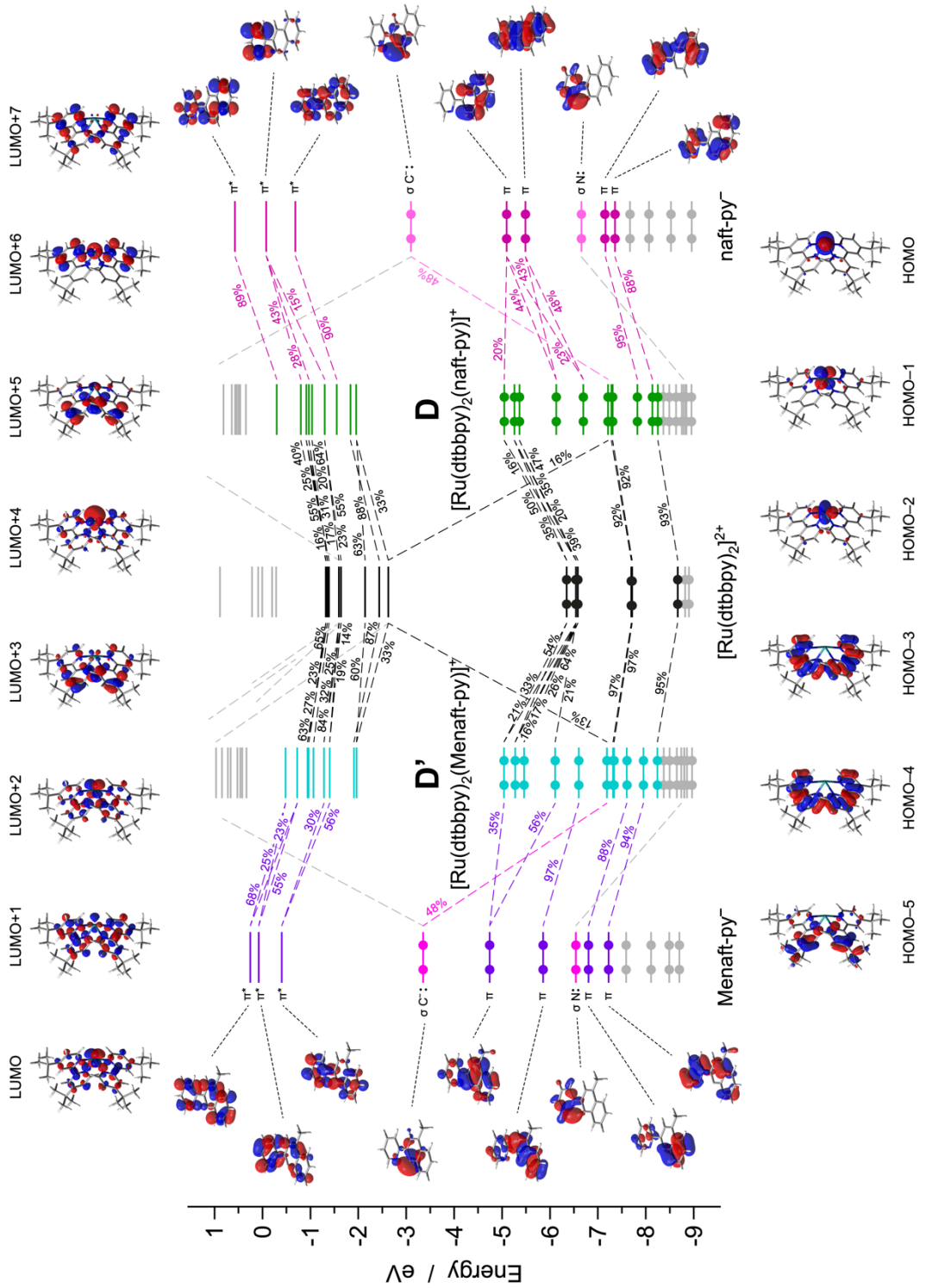


**Figure S28.** Orbital-interaction diagram of complexes **D** and **D'**, calculated in acetonitrile using charge decomposition analysis (see Experimental Section for further details). Fragment orbitals are computed by dividing each complex into 2 fragments: the shared $[Ru(dtbbpy)_2]^{2+}$ moiety and the third cyclometalating ligand (*i.e.*, the naft-py$^-$ unit for **D** and the methylated structural analogue in **D'**). The comparison is used to mainly assess the effect of the different cyclometalation position on the naphthyl fragment. Only fragment-orbital contributions above 10% are reported.

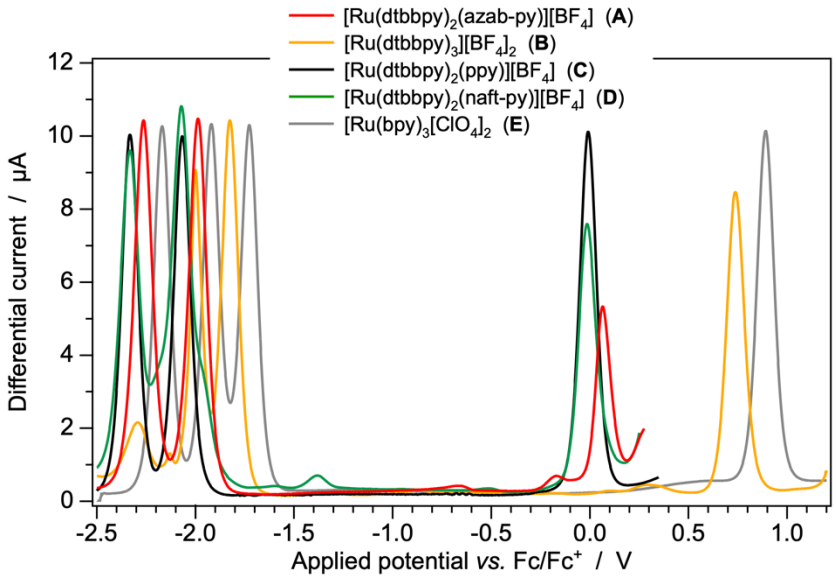


**Figure S29.** Square-wave voltammograms of complexes **A**–**D** and of reference compound **E** in acetonitrile solution at 298 K, recorded at a scan rate of 25 mV $s^{-1}$ with a square-wave amplitude of ±20 mV and a frequency of 25 Hz. Sample concentration is 1.0 mM.

**Table S1.** Comparison between electrochemical data from cyclic voltammetry (Table 1) and square-wave voltammetry in acetonitrile solution + 0.1 M $TBAPF_6$ at 298 K. All potential values are reported *vs.* the ferrocene/ferrocenium couple, used as internal reference.

| | *from square-wave voltammetry* | | *from cyclic voltammetry* | |
|---|---|---|---|---|
| | $E_{ox}$ [a] [V] | $E_{red}$ [a] [V] | $E_{ox}$ ($\Delta E_p$) [a] [V (mV)] | $E_{red}$ ($\Delta E_p$) [a] [V (mV)] |
| **A** | + 0.064 | – 1.988, – 2.264 | + 0.06 (irr.) | – 1.991 (70), – 2.262 (73) |
| **B** | + 0.739 | – 1.827 | + 0.735 (72) | – 1.825 (69) |
| **C** | – 0.009 | – 2.066, – 2.332 | – 0.009 (68) | – 2.071 (70), – 2.333 (67) |
| **D** | – 0.015 | – 2.071, – 2.333 | – 0.013 (73) | – 2.075 (77), – 2.328 (74) |
| **E** | + 0.891 | – 1.729, – 1.922, – 2.169 | + 0.889 (73) | – 1.730 (70), – 1.923 (73), – 2.172 (72) |

[a] The value in parenthesis is the peak-to-peak separation ($\Delta E_p$).

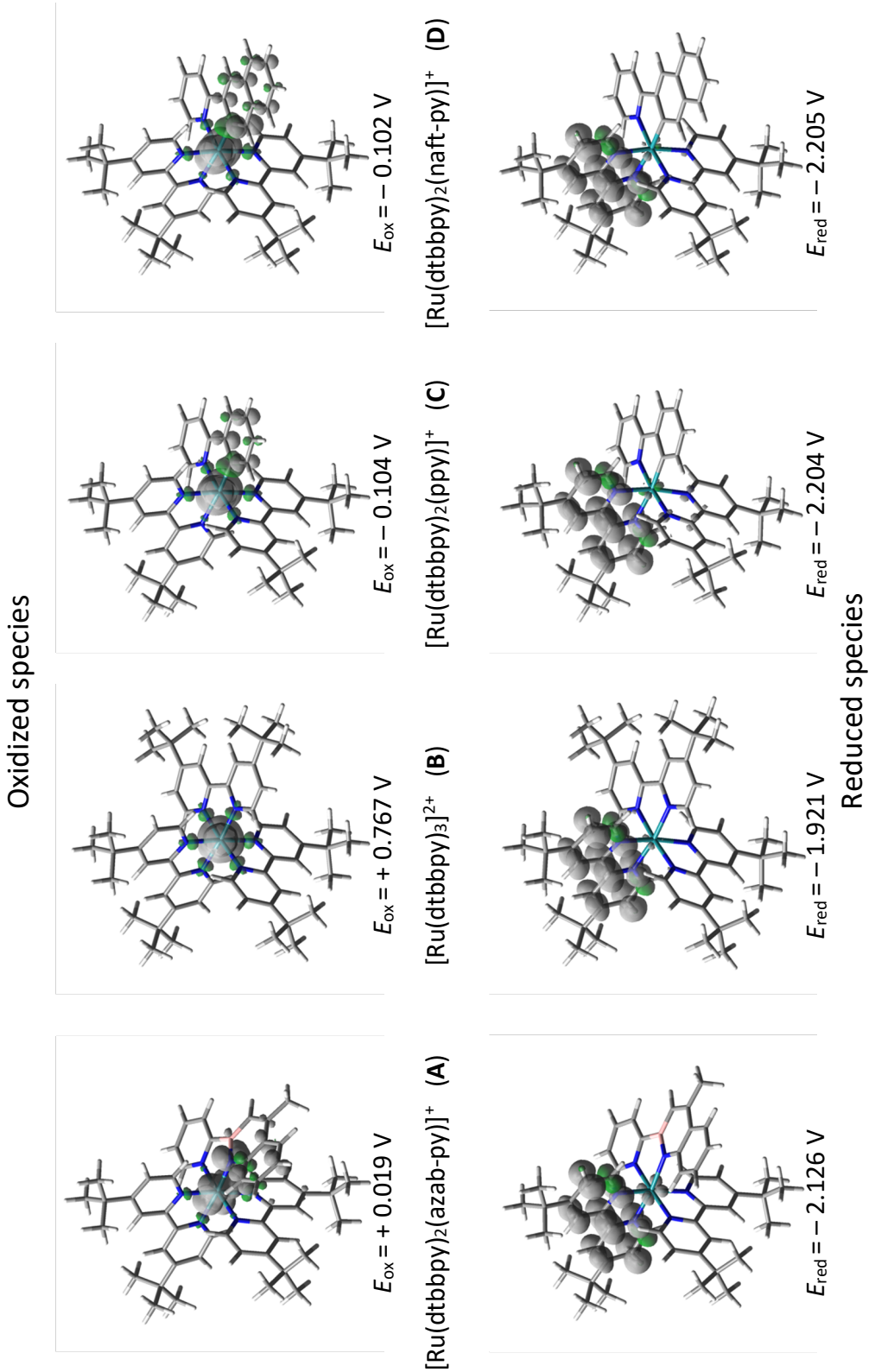


**Figure S30.** Spin-density distributions of the oxidized and reduced radicals of complexes **A**–**D** in their fully-relaxed geometries, computed by spin-unrestricted DFT in acetonitrile (isovalue: 0.002 e bohr$^{-3}$). The DFT-estimated redox potentials *vs.* the ferrocene/ferrocenium couple is also reported.

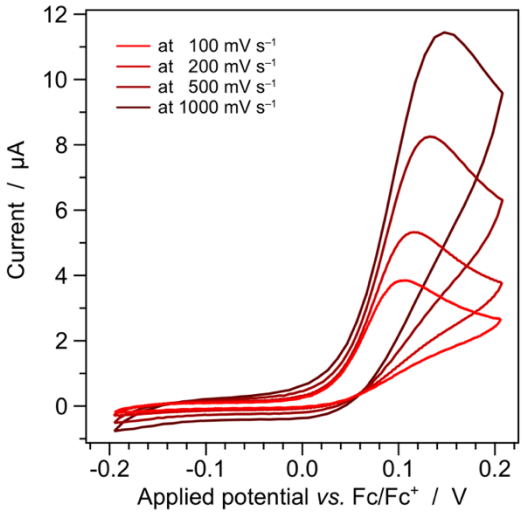


**Figure S31.** Anodic cyclic voltammograms of complex $[Ru(dtbbpy)_2(azab\text{-}py)]^+$ (**A**) at different scan rates in acetonitrile solution at 298 K (sample concentration: 1.0 mM). Experiments show the complete irreversibility of the oxidation process at any scan rate.

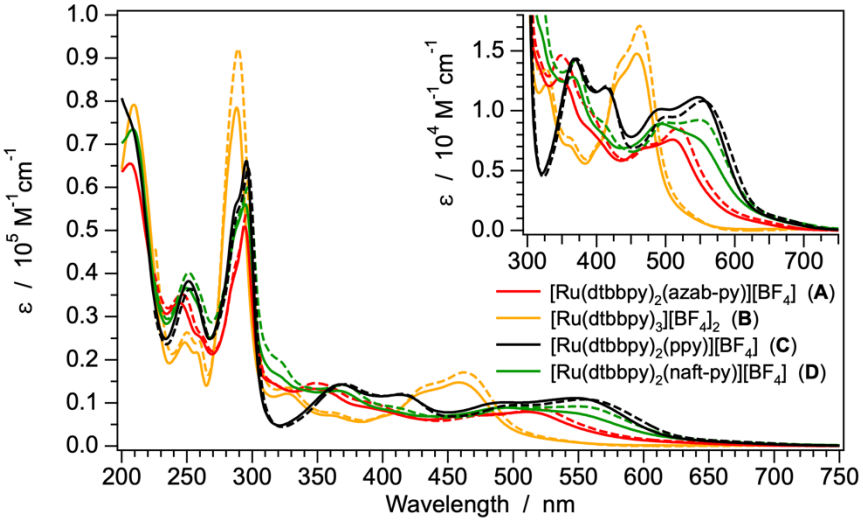


**Figure S32.** Comparison between the room-temperature absorption spectra of complexes **A**–**D** recorded in acetonitrile (full) and dichloromethane (dashed) solutions.

**Table S2.** Calculated NTOs couples describing the triplet excitations below 2.5 eV for $[Ru(dtbbpy)_2(azab\text{-}py)]^+$ (**A**) in acetonitrile. The λ value is the natural transition orbital eigenvalue associated with each NTOs {Motley, 2017, 13579-13592}{Motley, 2017, 13579-13592}couple; orbital isovalue: 0.04 $e^{-1/2}$ $bohr^{-3/2}$.

| | Transition energy [eV (nm)] | NTO couple hole → electron (λ) | Nature |
|---|---|---|---|
| $S_0 \rightarrow T_1$ | 1.90 (652) | 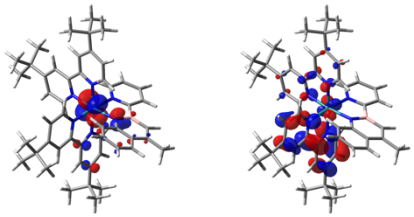 (96.3%) | $^3$MLCT from ruthenium to dtbbpy ligand |
| $S_0 \rightarrow T_2$ | 1.96 (634) | 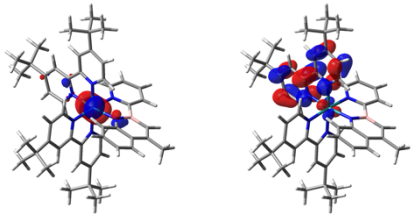 (74.1%) | $^3$MLCT from ruthenium to dtbbpy ligand |
| $S_0 \rightarrow T_3$ | 2.02 (612) | 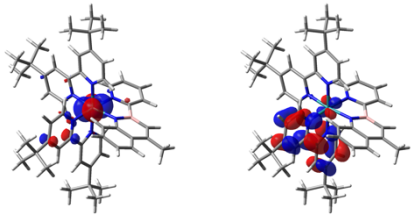 (76.4%) | $^3$MLCT from ruthenium to dtbbpy ligand |
| $S_0 \rightarrow T_4$ | 2.11 (589) | 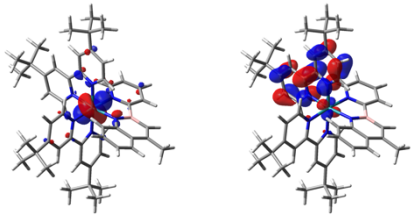 (95.3%) | $^3$MLCT from ruthenium to dtbbpy ligand |
| $S_0 \rightarrow T_5$ | 2.14 (580) | 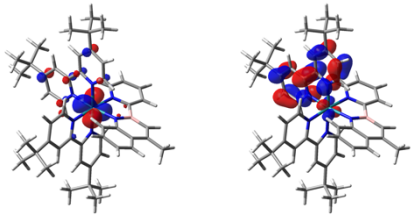 (84.7%) | $^3$MLCT from ruthenium to dtbbpy ligand |

| | | | | | |
|---|---|---|---|---|---|
| $S_0 \rightarrow T_6$ | 2.37 | (524) | 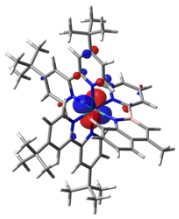 | 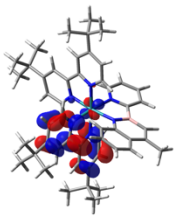 (96.8%) | $^3$MLCT from ruthenium to dtbbpy ligand |
| $S_0 \rightarrow T_7$ | 2.42 | (512) | 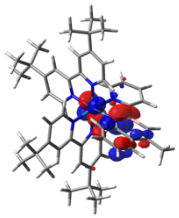 | 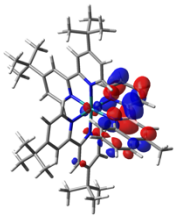 (90.5%) | mixed $^3$LC/$^3$MLCT involving the azaborine ligand and ruthenium ion |

**Table S3.** Calculated NTOs couples describing the triplet excitations below 2.5 eV for $[Ru(dtbbpy)_3]^{2+}$ (**B**) in acetonitrile. The λ value is the natural transition orbital eigenvalue associated with each NTOs couple; orbital isovalue: 0.04 $e^{-1/2}$ $bohr^{-3/2}$. State symmetry is also reported, accordingly to the $D_3$ point group.

| | Transition energy [eV (nm)] | NTO couple hole → electron (λ) | | Nature |
|---|---|---|---|---|
| $S_0 \rightarrow T_1$ (E) | 2.34 (530) | 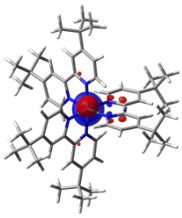 | 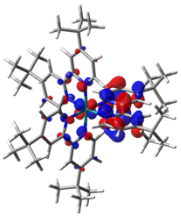 (93.0%) | $^3$MLCT from ruthenium to dtbbpy ligand |
| $S_0 \rightarrow T_2$ (E) | 2.34 (530) | 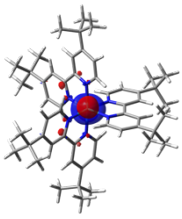 | 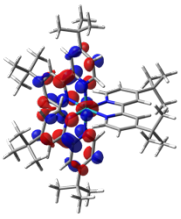 (92.9%) | $^3$MLCT from ruthenium to dtbbpy ligand |
| $S_0 \rightarrow T_3$ ($A_2$) | 2.36 (524) | 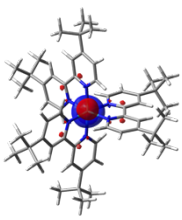 | 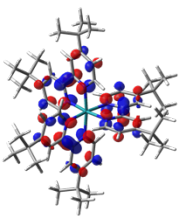 (89.0%) | $^3$MLCT from ruthenium to dtbbpy ligand |

| | | | | |
|---|---|---|---|---|
| $S_0 \rightarrow T_4$ ($A_2$) | 2.38 | (521) | 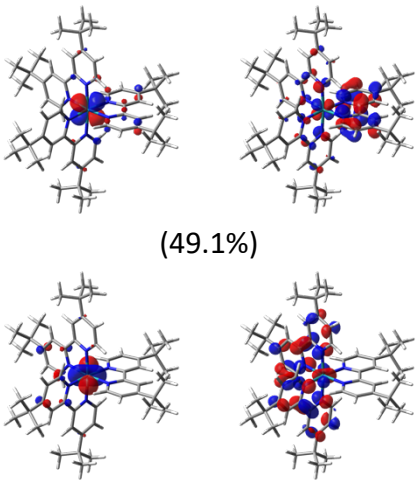 (49.1%) (49.1%) | $^3$MLCT from ruthenium to dtbbpy ligand |
| $S_0 \rightarrow T_5$ (E) | 2.47 | (502) | 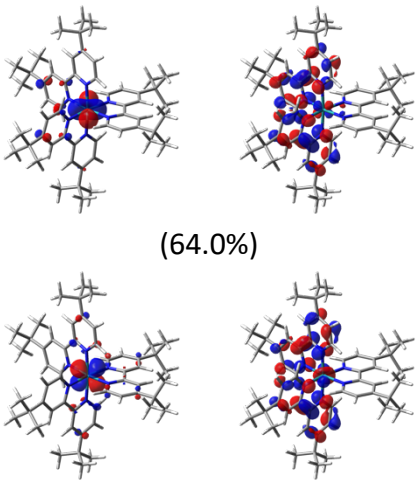 (64.0%) (34.1%) | $^3$MLCT from ruthenium to dtbbpy ligand |
| $S_0 \rightarrow T_7$ (E) | 2.47 | (502) | 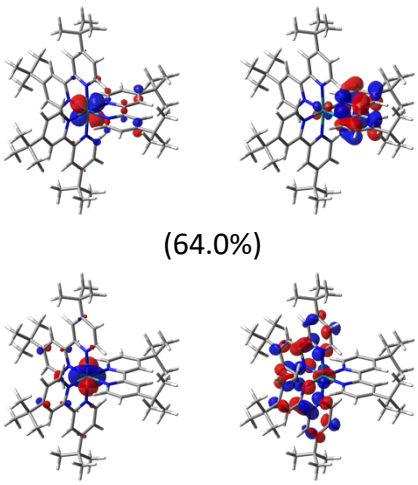 (64.0%) (34.1%) | $^3$MLCT from ruthenium to dtbbpy ligand |

**Table S4.** Calculated NTOs couples describing the triplet excitations below 2.5 eV for $[Ru(dtbbpy)_2(ppy)]^+$ (**C**) in acetonitrile. The λ value is the natural transition orbital eigenvalue associated with each NTOs couple; orbital isovalue: 0.04 $e^{-1/2}$ $bohr^{-3/2}$.

| | Transition energy [eV (nm)] | NTO couple hole → electron (λ) | Nature |
|---|---|---|---|
| $S_0 \rightarrow T_1$ | 1.83 (676) | 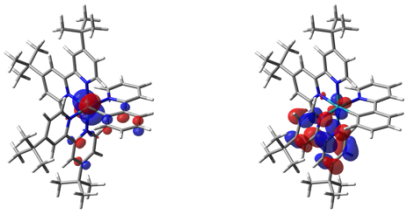 (98.3%) | $^3$MLCT from ruthenium to dtbbpy ligand |
| $S_0 \rightarrow T_2$ | 1.89 (657) | 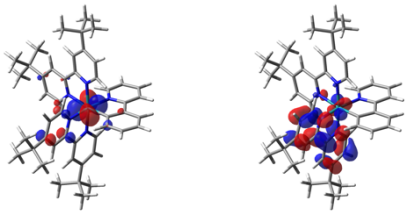 (95.5%) | $^3$MLCT from ruthenium to dtbbpy ligand |
| $S_0 \rightarrow T_3$ | 1.93 (641) | 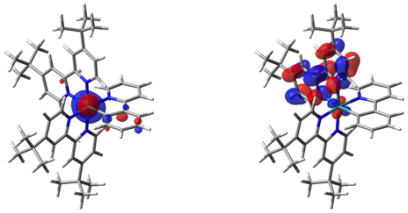 (97.6%) | $^3$MLCT from ruthenium to dtbbpy ligand |
| $S_0 \rightarrow T_4$ | 2.05 (605) | 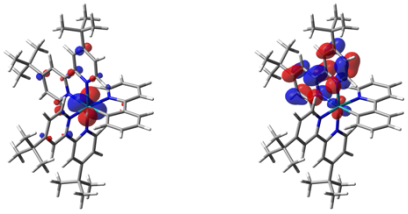 (89.9%) | $^3$MLCT from ruthenium to dtbbpy ligand |
| $S_0 \rightarrow T_5$ | 2.16 (574) | 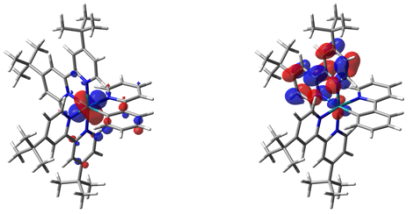 (98.3%) | $^3$MLCT from ruthenium to dtbbpy ligand |

| | | | | | |
|---|---|---|---|---|---|
| $S_0 \rightarrow T_6$ | 2.18 | (568) | 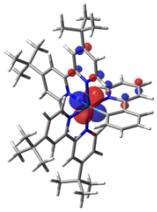 (99.3%) | 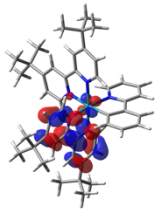 | $^3$MLCT from ruthenium to dtbbpy ligand |
| $S_0 \rightarrow T_7$ | 2.39 | (518) | 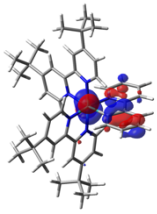 (96.8%) | 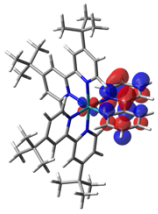 | {Motley, 2017, 13579-13592} |

**Table S5.** Calculated NTOs couples describing the triplet excitations below 2.5 eV for $[Ru(dtbbpy)_2(naft\text{-}py)]^+$ (**D**) in acetonitrile. The λ value is the natural transition orbital eigenvalue associated with each NTOs couple; orbital isovalue: 0.04 $e^{-1/2}$ $bohr^{-3/2}$.

| | Transition energy [eV (nm)] | NTO couple hole → electron (λ) | | Nature |
|---|---|---|---|---|
| $S_0 \rightarrow T_1$ | 1.83 (678) | 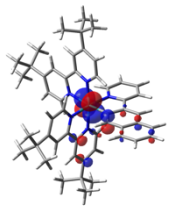 (98.2%) | 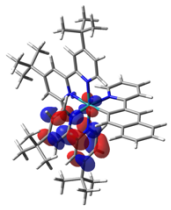 | $^3$MLCT from ruthenium to dtbbpy ligand |
| $S_0 \rightarrow T_2$ | 1.90 (653) | 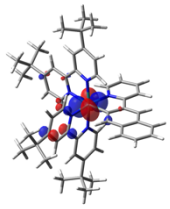 (94.2%) | 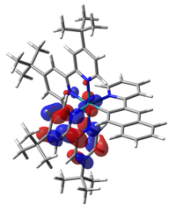 | $^3$MLCT from ruthenium to dtbbpy ligand |
| $S_0 \rightarrow T_3$ | 1.94 (639) | 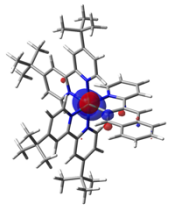 (94.6%) | 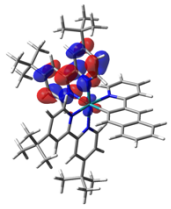 | $^3$MLCT from ruthenium to dtbbpy ligand |

| | | | | | |
|---|---|---|---|---|---|
| $S_0 \rightarrow T_4$ | 2.06 | (603) | 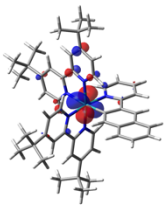 | 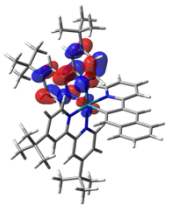 (88.9%) | $^3$MLCT from ruthenium to dtbbpy ligand |
| $S_0 \rightarrow T_5$ | 2.14 | (580) | 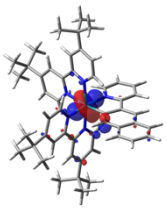 | 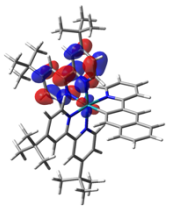 (98.4%) | $^3$MLCT from ruthenium to dtbbpy ligand |
| $S_0 \rightarrow T_6$ | 2.18 | (569) | 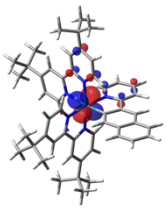 | 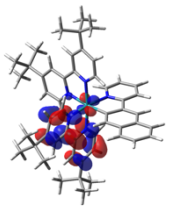 (98.6%) | $^3$MLCT from ruthenium to dtbbpy ligand |
| $S_0 \rightarrow T_7$ | 2.21 | (560) | 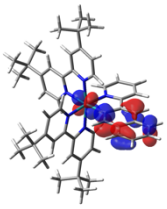 | 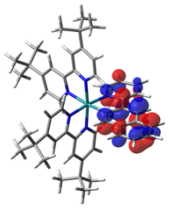 (93.6%) | mixed $^3$LC/$^3$MLCT involving the naft-py ligand and ruthenium ion |
| $S_0 \rightarrow T_8$ | 2.37 | (524) | 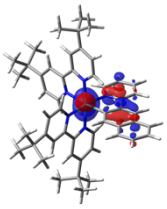 | 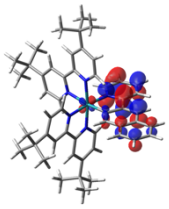 (92.7%) | mixed $^3$LC/$^3$MLCT involving the naft-py ligand and ruthenium ion |

**Table S6.** Calculated NTOs couples describing the triplet excitations below 2.5 eV for $[Ru(dtbbpy)_2(Me\text{-}naft\text{-}py)]^+$ (**D'**) in acetonitrile. The λ value is the natural transition orbital eigenvalue associated with each NTOs couple; orbital isovalue: 0.04 $e^{-1/2}$ $bohr^{-3/2}$.

| | Transition energy [eV (nm)] | NTO couple hole → electron (λ) | Nature |
|---|---|---|---|
| $S_0 \rightarrow T_1$ | 1.83 (678) | 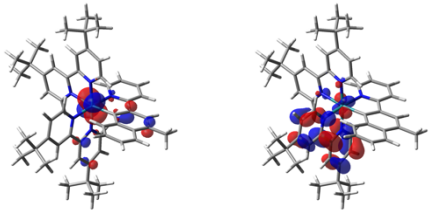 (97.6%) | $^3$MLCT from ruthenium to dtbbpy ligand |
| $S_0 \rightarrow T_2$ | 1.90 (654) | 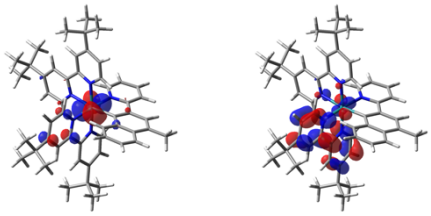 (95.3%) | $^3$MLCT from ruthenium to dtbbpy ligand |
| $S_0 \rightarrow T_3$ | 1.93 (643) | 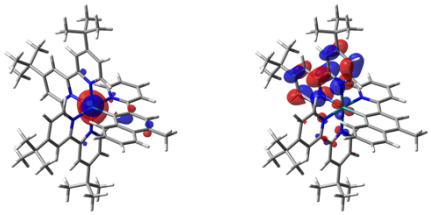 (96.4%) | $^3$MLCT from ruthenium to dtbbpy ligand |
| $S_0 \rightarrow T_4$ | 2.09 (594) | 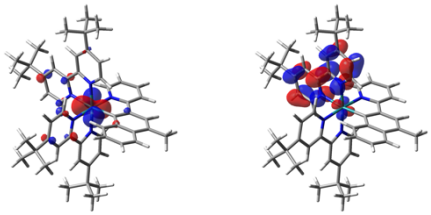 (78.9%) | $^3$MLCT from ruthenium to dtbbpy ligand |
| $S_0 \rightarrow T_5$ | 2.13 (583) | 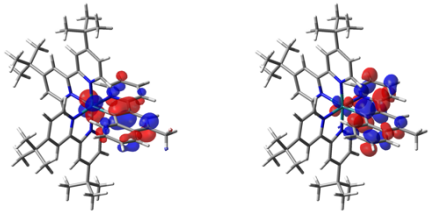 (82.3%) | mixed $^3$LC/$^3$MLCT involving the Me-naft-py ligand and ruthenium ion |

| | | | | | |
|---|---|---|---|---|---|
| $S_0 \rightarrow T_6$ | 2.13 | (581) | 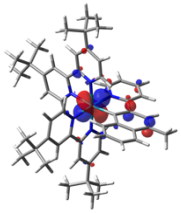 | 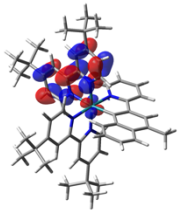 (96.6%) | $^3$MLCT from ruthenium to dtbbpy ligand |
| $S_0 \rightarrow T_7$ | 2.25 | (552) | 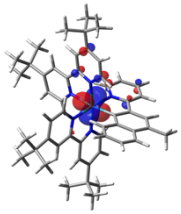 | 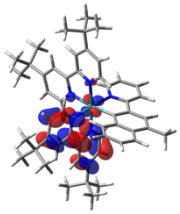 (98.8%) | $^3$MLCT from ruthenium to dtbbpy ligand |
| $S_0 \rightarrow T_8$ | 2.50 | (494) | 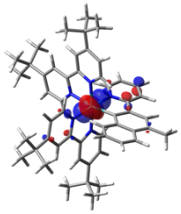 | 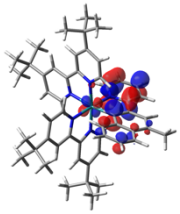 (95.7%) | mainly $^3$MLCT involving the naft-py ligand and ruthenium ion |

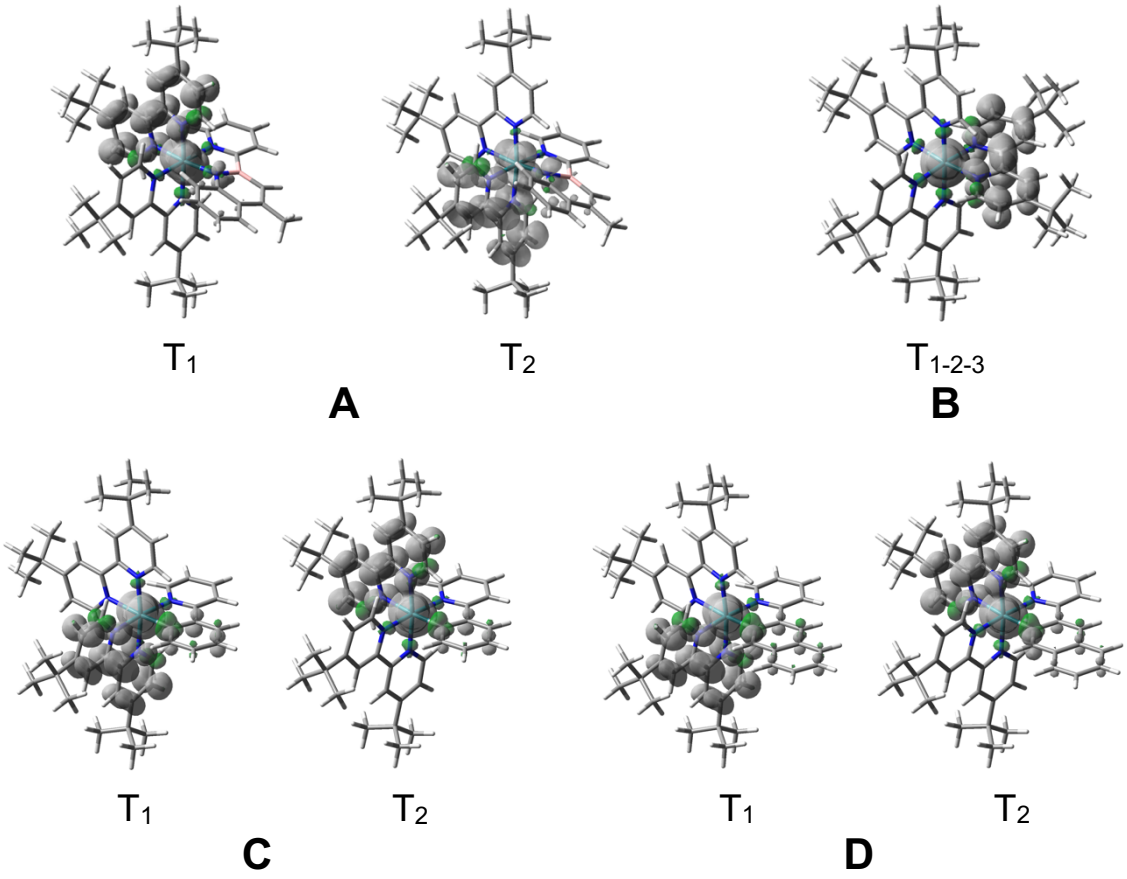


**Figure S33.** Spin-density distribution of the lowest triplet states of complexes **A**–**D** in their fully-optimized geometry, computed in acetonitrile (isovalues: 0.002 e bohr$^{-3}$). For all the complexes, the depicted triplets are $^3$MLCT in nature, formally involving the excitation of one electron from the ruthenium(II) centre to the π* orbitals of the dtbbpy ligands. Notably, two very close $^3$MLCT triplets ($T_1$ and $T_2$) are found in **A**, **C** and **D** due to the asymmetry of the azaborine or C^N ligand, removing the equivalency of the dtbbpy ligands (which, on the contrary, is preserved in **B**). The energy difference between such minima is only 9 meV for **A**, and 68 or 67 meV in the case of **C** or **D**.

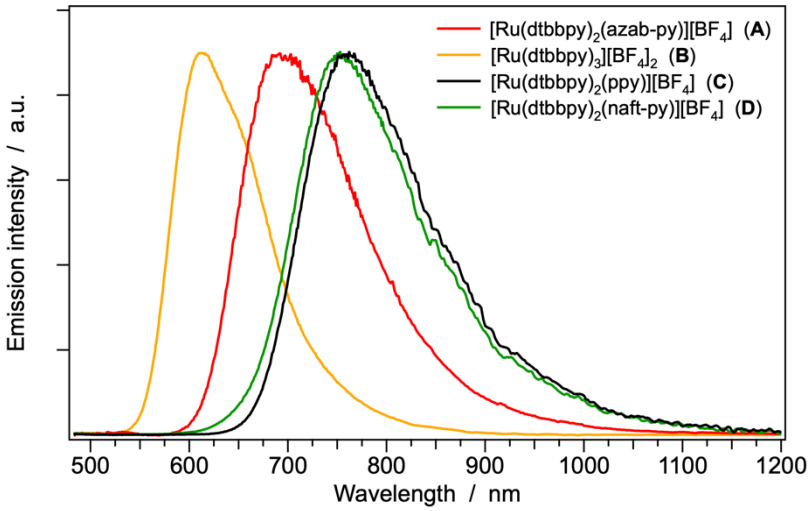


**Figure S34.** Normalized emission spectra of complexes **A**–**D** in 1% PMMA matrix at 298 K.